POLITECNICO DI TORINO
Repository ISTITUZIONALE

Design of Cycles by Impulsive Feedback: Application to Discrete Dosing

Original
Design of Cycles by Impulsive Feedback: Application to Discrete Dosing / Medvedev, A.V., Proskurnikov, A.V., Zhusubaliyev, Z.. - In: IEEE TRANSACTIONS ON CONTROL SYSTEMS TECHNOLOGY. - ISSN 1063-6536. - 34:6(2026), pp. 2984-2999. [10.1109/tcst.2026.3718511]

Availability:
This version is available at: 11583/3017043 since: 2026-10-26T22:22:59Z

Publisher:
IEEE

Published
DOI:10.1109/tcst.2026.3718511

Terms of use:

This article is made available under terms and conditions as specified in the corresponding bibliographic description in the repository

Publisher copyright
IEEE postprint/Author's Accepted Manuscript

©2026 IEEE. Personal use of this material is permitted. Permission from IEEE must be obtained for all other uses, in any current or future media, including reprinting/republishing this material for advertising or promotional purposes, creating new collecting works, for resale or lists, or reuse of any copyrighted component of this work in other works.

(Article begins on next page)

02 November 2026

Design of Cycles by Impulsive Feedback: Application to Discrete Dosing

Alexander V. Medvedev, Anton V. Proskurnikov, and Zhanybai Zhusubaliyev

***Abstract*—The task of maintaining a predefined level of effect in a dynamical plant by applying periodic control actions often arises in, e.g., process control and medicine. When the state variables of the plant represent the concentrations of chemical substances and the control action constitutes an instantaneous introduction of a certain quantity of a chemical or drug, this control setup is referred to as a (discrete) dosing problem. The present paper examines an amplitude- and frequency-modulated impulsive controller that, under stationary conditions, generates a desired sequence of uniform and equidistant control impulses based on continuous measurements of the output of a smooth positive nonlinear time-invariant single-input single-output plant with Wiener structure. The controller design method is based on constructing and stabilizing the fixed point of a discrete map that describes the evolution of the state vector of the continuous plant between successive impulsive control action instants. Stability of the fixed point ensures the existence of a basin of attraction around the stationary trajectory, where solutions of the closed-loop system converge to the stationary solution after perturbation. The convergence rate is determined by the slopes of the amplitude and frequency modulation functions of the impulsive controller. The proposed controller is applied to dosing of the drug *atracurium* in closed-loop neuromuscular blockade, and its performance is evaluated on a database of patient-specific pharmacokinetic-pharmacodynamic models estimated from clinical data. It is demonstrated that an implementation of the standard regimen as a pulse-modulated feedback controller significantly reduces the incidence of underdosing events.**

***Index Terms*—Nonlinear dynamical systems, amplitude modulation, frequency modulation, pulse modulation, medical control systems, anaesthesia.**

I. Introduction

An everyday example of a dosing application is adhering to a doctor's orders on a medication regimen, e.g., "take one tablet twice a day." This open-loop dosing strategy does not account for the actual medication effect in the particular patient. Typically, after initiating the treatment, the doctor evaluates the treated condition's symptoms in the patient and adjusts the regimen accordingly, thereby applying *feedback*.

The pharmacotherapy can be intensified in two ways: by increasing the amount of each single dose or by shortening the dosing interval. The choice between them essentially depends on pharmacological properties of the specific drug. Therefore, even manual administration of medication relies on at least a mental model of the drug's pharmacokinetics (PK) and pharmacodynamics (PD). Another useful observation from the conceptual example above is that the nominal regimen prescribes taking a tablet every twelve hours, which, when followed perfectly, results in a sequence of uniform and equidistant impulsive control actions sustained over an extended period.

Medication non-adherence poses a challenge in pharmacotherapy, impacting treatment outcomes and being difficult to manage [1]. A common patient concern is how to respond when a regular dose is delayed or missed. Clearly, the PK/PD properties of the drug should be considered in order to properly address the compliance lapse, as both dosing amounts and inter-dose intervals may need adjustment before resuming regular administration. A feedback controller can recommend corrective actions to the patient for timely regimen recovery, provided quantification of the drug effect is available.

Increasing or decreasing the amount of each dose corresponds to the mechanism of amplitude modulation in pulse-modulated control [2]–[4], whereas adjusting the dosing interval represents frequency modulation. The principles of amplitude and frequency modulation feedback implementing discrete dosing are widely employed in biological systems, e.g., in endocrine regulation [5]–[7].

Besides pharmacotherapies, where drugs are administered in tablet or injection form, similar discrete dosing problems – characterized by intermittent impulsive control actions and continuous effect measurements – are common in industrial processes. Examples include space technology, water treatment, food production, chemical and biochemical processes, agriculture, steelmaking and mining. This contrasts with continuous dosing, where the flow rate of a chemical is adjusted to achieve the desired effect. Industrial dosing control systems typically operate in open-loop mode and are implemented using discrete logic or automata [8]. An early example of applying optimal control to dosing can be found in R. Bellman's work [9]. However, open-loop control cannot mitigate the effects of disturbances and model uncertainty in the plant, which necessitates the use of feedback in dosing.

Impulsive feedback control is inherently nonlinear. Integrating advanced control laws into closed-loop dynamics adds layers of complexity, making the stability and performance analysis of the resulting system challenging. However, until recently, simple pulse-modulated feedback solutions manipulating the amplitude and frequency of the control impulses have been notably absent. The preferred method for designing impulsive feedback is currently Model Predictive Control

Alexander V. Medvedev [alexander.medvedev@it.uu.se] is with Department of Information Technology, Uppsala University, SE-752 37 Uppsala, Sweden.

Anton V. Proskurnikov [anton.p.1982@ieee.org] is with Department of Electronics and Telecommunications, Politecnico di Torino, Turin, Italy, 10129.

Zhanybai T. Zhusubaliyev [zhanybai@hotmail.com] is with Department of Computer Science, International Scientific Laboratory for Dynamics of Non-Smooth Systems, Southwest State University, Kursk, Russia and Faculty of Mathematics and Information Technology, Osh State University, Lenin st. 331, 723500, Osh, Kyrgyzstan.

(MPC). Motivated by a drug-dosing application and an available PK/PD model, an MPC with impulsive control action was proposed in [10]. A promising application of impulsive MPC to insulin dosing in simulated diabetes patients is reported in [11], [12]. The physiological profile of insulin secretion includes around ten major hormone pulses over 24 hours [13], whose timing is closely related to meal times.

This paper develops and evaluates a new framework for impulsive dosing control design, hinging on the findings in recent conference papers [14]–[16]. The latter publications demonstrate that a nonlinear amplitude and frequency pulse modulator can be designed to control a positive continuous linear time-invariant third-order plant to a specified periodic solution. By reducing the hybrid system dynamics to a discrete nonlinear map, the local transient properties of the closed-loop system are determined by the location of the multipliers of the fixed point corresponding to the stationary periodic solution. It is readily observed that the structure of the closed-loop system is identical to that of the Impulsive Goodwin's Oscillator (IGO), a mathematical model of pulsatile endocrine regulation [17]–[19]. Therefore, the pulse-modulated controller considered further in this paper can be seen as biomimetic.

The application illustrating the utility of the proposed framework is neuromuscular blockade (NMB) during anesthesia. NMB causes skeletal muscle relaxation and is routinely used in anesthesia to optimize surgical conditions. NMB drugs can be administered either in intermittent doses or through continuous infusion. Following an initial bolus dose, sequential maintenance doses or a certain infusion rate are necessary to sustain anesthesia. Underdosing NMB can lead to inadequate paralysis, while overdosage may extend neuromuscular block beyond the time necessary for surgery and anesthesia. The effect of NMB agents is measured by neuromuscular monitors [20], devices that electrically stimulate a peripheral nerve while also quantifying the evoked responses. Compared to administration of fixed doses (open-loop control), using the monitors for dose titration significantly reduces exposure to NMB drugs without affecting the observed clinical outcome [21].

The long-term (one to ten days) NMB is practiced during mechanical ventilation in the intensive care unit. It has become especially common in connection with treatment for COVID-19 during inpatient hospitalization [22]. There is wide interpatient variability in required NMB agent dosage and the latter may decrease or increase with time. To ensure optimal dosing, it is therefore important to monitor the depth of NMB under constant flow rate infusion.

Closed-loop control of NMB was addressed early in the development of automatic anesthesia since the plant is single-input single-output and the PK are uncomplicated. When a patient-specific PK/PD model is available, the controller design problem is not challenging, particularly for maintaining NMB after the initial bolus dose is administered in open loop. For instance, relay control is reported to handle closed-loop NMB drug administration effectively, ensuring performance appropriate for surgery [23]. This highlights an important feature of closed-loop drug delivery: Control performance is irrelevant unless it translates into a clinical effect. In [24], patient variability with respect to NMB drugs is identified as the main challenge in closed-loop administration. This issue is addressed by integrating patient-specific control with the support of online system identification of the nonlinear PK/PD model. The same paper also discusses the limitations of using a fixed PID controller, noting that it fails to deliver adequate performance given the model uncertainty. As shown in [25], besides nonlinear oscillations (limit cycles) typical of PID stabilization control of nonlinear systems, deterministic chaos can arise in the closed-loop NMB at lower concentrations of the anesthetic drug. Based on bifurcation analysis, a systematic approach to online recovery from oscillations is proposed and evaluated in simulation in [26].

The main contribution of the present paper is analysis of a pulse-modulated controller suggested in [14] and its specialization to a realistic drug dosing problem. An analytic expression for the fixed point corresponding to a desired periodic solution of the closed-loop system is provided in Theorem 1. An orbital stability condition for the periodic solution in terms of the slopes of the modulation functions is provided in Theorem 2. This theorem also provides an upper bound for the achievable convergence rate to the periodic solution under perturbation. Being evaluated over a population of Wiener-structured PK/PD NMB models estimated from clinical data, a pulse-modulated dosing controller designed for the population mean model parameters is shown to exhibit acceptable performance and robustness. It also significantly improves the incidence of NMB agent underdosing events compared to open-loop administration.

The rest of the paper is organized as follows. Section II introduces the mathematical model of NMB employed to analyze the properties of the impulsive feedback controller along with the dataset underlying the numerical experiments in this study. The controller design problem at hand is mathematically formulated in Section III, and the necessary background in non-smooth dynamical systems is provided in Section IV. An evaluation of controller performance and robustness on a realistic cohort of synthetic NMB patients is presented in Section V. Conclusions are drawn in Section VI, followed by appendices with the proofs of the theorems and lemmas.

II. Neuromuscular blockade model

A continuous-time Wiener model for NMB with the muscle relaxant *atracurium* under general closed-loop anesthesia is introduced in [27]. The model assumes continuous infusion of the drug and the input $u(t)$ is the administered atracurium rate in $[\mu\text{g kg}^{-1}\text{min}^{-1}]$, positive and bounded: $0 \leq u(t) \leq u_{\max}$. The bolus dose administered to a patient in the induction phase is translated in the identification dataset to an equivalent flow over a short time interval. The current NMB level determines the model output $y(t)$ [%], which is measured by a train-of-four monitor (a peripheral nerve stimulator). The maximal level of output $y(t) = 100\%$ is achieved at the instant when the NMB is initiated and there is no drug in the bloodstream.

A. Continuous-time Wiener PK/PD model

The PK model part is assumed to be linear and time-invariant, with a rational transfer function from the input $u(t)$ to the serum drug concentration $\bar{y}(t)$ defined as follows

$$W(s) = \frac{\bar{Y}(s)}{U(s)} = \frac{v_1 v_2 v_3 \alpha^3}{(s + v_1\alpha)(s + v_2\alpha)(s + v_3\alpha)}. \quad (1)$$

Here $\bar{Y}(s) = \mathcal{L}\{\bar{y}(t)\}$, $U(s) = \mathcal{L}\{u(t)\}$, and $\mathcal{L}\{\cdot\}$ denotes the Laplace transform. The parameter $0 < \alpha \leq 0.1$ is patient-specific and estimated from data, whereas the other parameters in (1) are fixed: $v_1 = 1$, $v_2 = 4$, and $v_3 = 10$. The pole spectrum of (1) is scaled linearly with α, and the static gain is adjusted to one. The PD part of the NMB model output is static and relates the output of (1) to the measured by the monitor effect through a nonlinear Hill-type function

$$y(t) = \varphi(\bar{y}(t)), \quad \text{where} \quad \varphi(z) \triangleq \frac{100C_{50}^{\gamma}}{C_{50}^{\gamma} + z^{\gamma}(t)}, \tag{2}$$

where $C_{50} = 3.2425$ μg ml^{-1} is the drug concentration that produces 50% of the maximum effect, and $0 < \gamma \leq 10$ is a patient-specific parameter. With model in (1), (2), the effect of the NMB agent on the patient is captured by a pair (α, γ).

A state-space realization of Wiener model (1), (2) is

$$\dot{x}(t) = Ax(t) + Bu(t), \ \bar{y}(t) = Cx(t), \ y(t) = \varphi(\bar{y}(t)), \tag{3}$$

where the coefficients of the linear part are

$$A = \begin{bmatrix} -a_1 & 0 & 0 \\ g_1 & -a_2 & 0 \\ 0 & g_2 & -a_3 \end{bmatrix}, B = \begin{bmatrix} 1 \\ 0 \\ 0 \end{bmatrix}, C^{\top} = \begin{bmatrix} 0 \\ 0 \\ 1 \end{bmatrix}, \tag{4}$$
$$a_1 \triangleq v_1\alpha, a_2 \triangleq v_2\alpha, a_3 \triangleq v_3\alpha, g_1 \triangleq v_1\alpha, g_2 \triangleq v_2v_3\alpha^2,$$

and the state variables are $x = [x_1, x_2, x_3]^{\top}$.

It is readily observed that the matrix A is Hurwitz and Metzler. The asymptotic stability of the linear part in (3) aligns with the natural decay of chemical substances over time, and the positivity of x ensures that the state variables can be interpreted as concentrations. The chain structure of the linear part represents the dynamics of the sequential PK/PD model compartments, and the state variables correspond to drug concentrations in each compartment. The function $\varphi(\cdot)$ is smooth, positive, and bounded.

B. Dataset

The dataset used in this study is described in detail in [27]. It was further employed in [28] to compare the performance of two recursive parameter estimation techniques, namely, the Extended Kalman Filter (EKF) and the Particle Filter, on clinical data with respect to the NMB model described in Section II. The dynamics of closed-loop controllers based on this model are investigated in [25] and [29].

The model parameter estimates for 48 patients are illustrated in Fig. 1. The population mean parameter values are $\bar{\alpha} = 0.0374, \bar{\gamma} = 2.6677$. The PK parameter α varies by 48% across the dataset, whereas the PD parameter γ varies by nearly 75%. Given the nonlinear character of the PD, the latter uncertainty is the most challenging one. The correlation between the estimates of α and γ is low, as seen in Fig. 2. However, models with extreme values of γ do not exhibit high values of α, and high values of both parameters are not observed at all. In contrast, the model with Patient Identification Number (PIN) 26 features the lowest value of γ and the highest value of α.

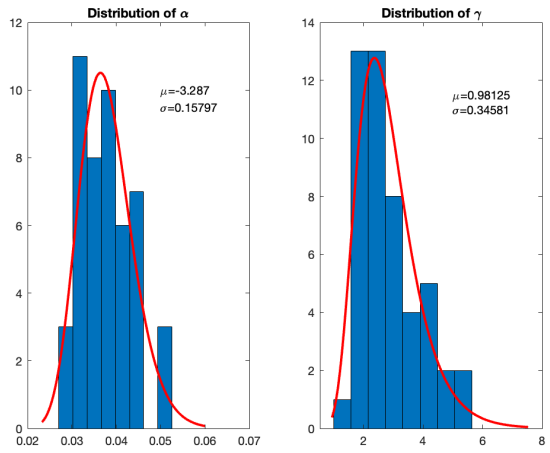


Fig. 1: Histograms (blue) and estimated lognormal distributions (red) for the model parameters in the data set. Lognormal distribution is selected due to the positivity of the model parameters (α, γ).

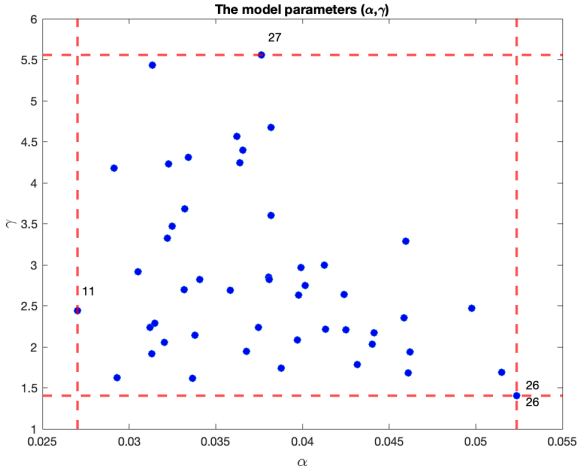


Fig. 2: The model parameter pairs (α, γ) in the dataset: $\alpha_{\min} = 0.0270 \leq \alpha \leq 0.0524 = \alpha_{\max}$, $\gamma_{\min} = 1.4030 \leq \gamma \leq 5.5619 = \gamma_{\max}$. The extreme parameter values are indicated by the Patient Identification Number.

III. Problem Formulation

In what follows, the continuous plant in (3) is controlled by an impulsive output feedback, characterized by frequency and amplitude pulse modulation operators [2]. This control action can be described as an infinite sequence of Dirac delta-functions fed as input to the linear block (3), $u(t) = \sum_{n=0}^{\infty} \lambda_n \delta(t - t_n)$, where the weights and firing times of the impulses depend on the nonlinear plant output y. Equivalently, the effect of impulses is represented by instantaneous jumps in the state vector, whose timing is governed by a difference

equation. This leads to the following hybrid dynamics:

$$\begin{aligned} \dot{x}(t) &= Ax(t), \quad t \in (t_n, t_{n+1}), \\ x(t_n^+) &= x(t_n^-) + \lambda_n B, \quad x(0^-) = x_0, \\ t_{n+1} &= t_n + T_n, \quad t_0 = 0, \\ T_n &= \bar{\Phi}(y(t_n)), \ \lambda_n = \bar{F}(y(t_n)), \end{aligned} \tag{5}$$

where $n = 0, 1, \ldots$ and the output $y(t)$ is defined in (3). The minus and plus in a superscript in (5) denote the left-sided and right-sided limits, respectively. The instants t_n are termed (impulse) firing times, and λ_n represents the corresponding impulse weight. Despite the jumps in (5), $y(t)$ and $\bar{y}(t)$ remain smooth since $\varphi(\cdot)$ is smooth and

$$CB = CAB = 0, \, CA^2B \neq 0, \tag{6}$$

rendering the linear block a system of relative degree 2.

The *design degrees of freedom* of the impulsive controller in question are the frequency modulation function $\bar{\Phi}(\cdot)$ and the amplitude modulation function $\bar{F}(\cdot)$.

With $\circ$ denoting composition, introduce the functions

$$\Phi(\cdot) \triangleq (\bar{\Phi} \circ \varphi)(\cdot), \quad F(\cdot) \triangleq (\bar{F} \circ \varphi)(\cdot). \tag{7}$$

The following restrictions on the design degrees of freedom are imposed. Both $F(\cdot)$ and $\Phi(\cdot)$ are assumed to be continuous and monotonic, with $F(\cdot)$ being nonincreasing and $\Phi(\cdot)$ being nondecreasing on $[0, \infty)$. To guarantee boundedness of closed-loop solutions in (3), (5), it is required that

$$0 < \Phi_1 \leq \Phi(\cdot) \leq \Phi_2, \quad 0 < F_1 \leq F(\cdot) \leq F_2, \tag{8}$$

where Φ_1, Φ_2, F_1, F_2 are constants.

Control Problem: The problem at hand is to select the modulation functions $\bar{\Phi}(\cdot)$, $\bar{F}(\cdot)$ so that the closed-loop system (5) exhibits an orbitally stable periodic solution with a predefined period $T > 0$ and a given pulse weight $\lambda > 0$, i.e., a solution with $\lambda_n \equiv \lambda$, $T_n \equiv T$, for all n.

IV. Closed-loop dynamics and 1-cycles

Under the assumptions introduced in the previous section and with the plant nonlinearity φ incorporated in the modulation functions Φ and F, the closed-loop system (5) is identical to the Impulsive Goodwin's Oscillator (IGO) [17], [18], a hybrid mathematical model originally devised to describe pulsatile endocrine regulation. Denoting $X_n = x(t_n^-)$, the state vector sequence of the IGO obeys the impulse-to-impulse (or *return*) map [18], [30] as follows:

$$\begin{aligned} X_{n+1} &= Q(X_n), \\ Q(\xi) &\triangleq \mathrm{e}^{A\Phi(C\xi)} \left(\xi + F(C\xi)B\right). \end{aligned} \tag{9}$$

Between the firing instants, the continuous state trajectory on the interval (t_n, t_{n+1}) is uniquely defined by X_n as

$$x(t) = \mathrm{e}^{(t-t_n)A}(X_n + \lambda_n B), \quad t \in (t_n, t_{n+1}). \tag{10}$$

A. The fixed point and 1-cycle

As shown in [18], the mapping Q has a unique fixed point

$$X = Q(X), \tag{11}$$

for every pair of the nonlinear functions F, Φ in (7) that are, respectively, nonincreasing and nondecreasing, and obey (8). This fixed point determines a special type of periodic solution, termed *1-cycle* [30], [31] and characterized by only one firing of the feedback in the (least) period. Denoting $\bar{y}_0 \triangleq CX$, the 1-cycle is uniquely determined by the solution of (11) and obtained by substituting $x(t_n^-) = X_n = X$, $T_n = T \triangleq \Phi(\bar{y}_0)$, and $\lambda_n = \lambda \triangleq F(\bar{y}_0)$ into (10) (then, obviously, $X_{n+1} = Q(X) = X = X_n$, so that the hybrid solution is T-periodic).

Using the Opitz formula [32], [33] from matrix calculus, the solution of (11) with the given parameters λ and T can be found explicitly by using divided differences. The first divided difference of a function $h(\cdot)$ is defined as

$$h[x_1, x_2] \triangleq \frac{h(x_1) - h(x_2)}{x_1 - x_2},$$

and higher-order divided differences are defined recursively by

$$h[x_0, \ldots, x_k] = \frac{h[x_1, \ldots, x_k] - h[x_0, \ldots, x_{k-1}]}{x_k - x_0}.$$

Here, for simplicity, only distinct points $x_i \neq x_j$ are considered; a general definition can be found in [33].

A closed-form expression of the desired fixed point is provided in the next theorem.

Theorem 1. *Let $\lambda, T > 0$ be fixed and $\mu(x) \triangleq \frac{1}{\mathrm{e}^{-x} - 1}$. Then, the following statements are equivalent:*

1) X and $\bar{y}_0 = CX$ obey the equations

$$X = \lambda \begin{pmatrix} \mu(-a_1 T) \\ g_1 \mu[-a_1 T, -a_2 T] \\ g_1 g_2 \mu[-a_1 T, -a_2 T, -a_3 T] \end{pmatrix}, \tag{12}$$

$$\Phi(\bar{y}_0) = T, \quad F(\bar{y}_0) = \lambda, \tag{13}$$

where a_i, g_i are defined in (4).

2) $X > 0$ is the fixed point of the map $Q(\cdot)$ that corresponds to 1-cycle of the period T and with the pulse weight λ.

Proof. See Appendix B. □

Substituting the expressions for a_i, g_i from (4), Fig. 3 illustrates the dependence of the fixed point X in (12) on α for a pair of parameters (λ, T). It can be shown that for each $T > 0$ the components are decreasing functions of α.

Theorem 1 suggests a method for designing the nonlinearities F and Φ in such a way as to guarantee the existence of a 1-cycle with predefined parameters λ, T for a given value of α. It suffices to calculate the fixed point X according to (12), and then find F, Φ in such a way that (13) holds. However ensuring a sustained 1-cycle requires orbital stability. A complete controller design algorithm is provided in Section V-B.

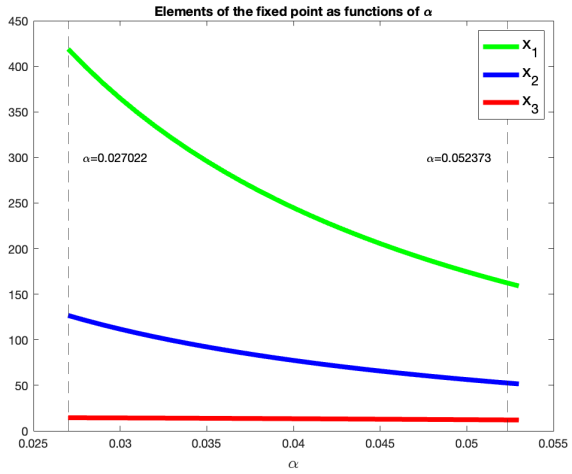


Fig. 3: Fixed point coordinates as functions of $\alpha \in [\alpha_{\min}, \alpha_{\max}]$ for $\lambda = 200$ and $T = 20$.

B. The Jacobian of the return map at the fixed point

To sustain the desired periodic solution in the closed-loop system (3), (5), the 1-cycle has to be orbitally stable, which property is guaranteed by stability of the corresponding fixed point. To test stability of the 1-cycle, the Jacobian of the pointwise map $Q(\cdot)$ is evaluated at the fixed point X. A straightforward computation shows [14] that

$$\begin{aligned} Q'(X) &= \mathrm{e}^{A\Phi(\bar{y}_0)} + (F'(\bar{y}_0)J + \Phi'(\bar{y}_0)D)\,C, \\ D \triangleq AX &= F(\bar{y}_0)A(\mathrm{e}^{-A\Phi(\bar{y}_0)} - I)^{-1}B, \\ J &\triangleq \mathrm{e}^{A\Phi(\bar{y}_0)}\,B. \end{aligned} \tag{14}$$

The 1-cycle corresponding to the fixed point X is orbitally stable when the matrix $Q'(X)$ is Schur.

Now the control problem from Section III can be reformulated in terms of fixed point.

Control Problem (Reformulation): Given the plant (3) and the desired parameters of the periodic solution, λ and T, find the modulation functions $\bar{\Phi}(\cdot)$ and $\bar{F}(\cdot)$ such that the fixed point (12) solves (13) and renders $Q'(X)$ Schur-stable.

a) Trivial Solution: Periodic Open-Loop Control: It can be noted that stability of the 1-cycle can be achieved without the impulsive feedback (5), by choosing constant modulation functions $F(\cdot) \equiv \lambda$ and $\Phi(\cdot) \equiv T$. In this case, $Q'(X) = \mathrm{e}^{TA}$ by (14). Since A is Hurwitz, e^{TA} is Schur stable, with spectral radius $\rho(\mathrm{e}^{AT}) = \mathrm{e}^{-a_1 T} = \mathrm{e}^{-\alpha v_1 T}$, using $0 < a_1 < a_2 < a_3$. This configuration effectively drives (3) in open-loop mode with a train of equidistant impulses of constant weight.

However, impulsive feedback plays a crucial role in enhancing convergence to the desired periodic solution in the presence of deviations. In particular, nonzero slopes $F'(\bar{y}_0)$ and $\Phi'(\bar{y}_0)$ allow the spectral radius $\rho(Q'(X))$ to be reduced.

b) Relation to Static Output Stabilization: Notice that selecting $F'(\bar{y}_0)$ and $\Phi'(\bar{y}_0)$ to stabilize the fixed point X is equivalent to finding a gain K that renders the matrix

$$Q'(X) = A_\Phi + WKC \tag{15}$$

Schur stable, where we denote

$$A_\Phi \triangleq \mathrm{e}^{A\Phi(\bar{y}_0)}, W \triangleq \begin{bmatrix} J & D \end{bmatrix}, K^\top \triangleq \begin{bmatrix} F'(\bar{y}_0) & \Phi'(\bar{y}_0) \end{bmatrix}.$$

This problem corresponds to stabilization of a discrete-time system

$$\begin{aligned} x_d(t+1) &= A_d x_d(t) + B_d u_d(t), \\ y_d(t) &= C_d x_d(t), \end{aligned}$$

by the output feedback $u_d(t) = K_d y_d(t)$. The closed-loop system is stable when the matrix $A_d + B_d K_d C_d$ is Schur. The problem of finding such a matrix K_d is known as (static) output feedback stabilization; see [34] for a review. An additional constraint imposed by the impulsive Goodwin oscillator structure is that the elements of the matrix K are sign-definite, $K_1 \le 0$ and $K_2 \ge 0$, in view of the monotonicity properties of F and Φ.

It is known that the general static output feedback stabilization problem reduces to the feasibility of a nonconvex quadratic matrix inequality [34]. The special structure of the three-dimensional system considered here allows an *analytic* characterization of all pairs of slope tangents $(\Phi'(\bar{y}_0), F'(\bar{y}_0))$ that ensure orbital stability of the 1-cycle corresponding to the parameters $F(\bar{y}_0) = \lambda$ and $\Phi(\bar{y}_0) = T$. Such a characterization is provided by Theorem 2 in the next section.

c) Impulsive Control as a Local Negative Feedback: The stability criterion derived in the next section is based on the following property of the pulse-modulated feedback (5), which is of independent interest.

Lemma 1. *The vectors D and J in (14) obey the inequalities*[1]

$$D < 0 \;\; \textit{and} \;\; J > 0.$$

Proof. See Appendix B. □

Together with the monotonicity assumptions on the modulation functions, Lemma 1 entails

$$JF'(\bar{y}_0) + D\Phi'(\bar{y}_0) < 0, \tag{16}$$

for all values of the tangent slopes $F'(\bar{y}_0) \le 0$ and $\Phi'(\bar{y}_0) \ge 0$, one of which is nonzero. Recalling the analogy with the output feedback stabilization problem, inequality (16) highlights the role of the pulse-modulated feedback (5) as negative feedback with respect to the linear block output $\bar{y}(t)$. This is a principal property of the closed-loop system (3), (5), since all signals involved are positive, while the negative feedback principle is implemented in a well-defined mathematical sense. In view of the underlying endocrine regulation problem modeled by the IGO, the impulsive control approach considered here provides a formal explanation of how biofeedback operates.

From (14) and (16), it also follows that increasing $\Phi'(\bar{y}_0)$ and decreasing $F'(\bar{y}_0)$ may eventually lead to loss of stability, as some eigenvalues of $Q'(X)$ increase in absolute value. While no analytic expression for the spectral radius of $Q'(X)$ as a function of the tangent slopes is available, we provide its numerical analysis in Subsection IV-D.

[1] All inequalities involving vectors are understood elementwise.

C. The Schur Stability Criterion

Although the expression for the spectral radius of the Jacobian matrix (14) is complicated, an analytic necessary and sufficient condition on the slopes of the modulation functions that ensures $Q'(X)$ is Schur stable does exist. Unlike the standard Jury and Schur–Cohn criteria for stability of a general third-order polynomial, the stability conditions derived below are *linear* with respect to the slope coefficient $F'(\bar{y}_0)$. Due to the structure of the Jacobian (14), we address the following.

Stability Problem: Find all real pairs $(\xi \le 0, \eta \ge 0)$ such that $\mathscr{Q}(\xi,\eta)$ is Schur stable, where

$$\mathscr{Q}(\xi,\eta) \triangleq \mathrm{e}^{AT} + (\xi J + \eta D)\, C. \tag{17}$$

To formulate the conditions for Schur stability, we introduce the functions

$$\begin{aligned}\psi(s|\xi,\eta) &\triangleq \frac{\det\left(sI - \mathscr{Q}(\xi,\eta)\right)}{\det(sI - \mathrm{e}^{AT})} \\ &= 1 - C(sI - \mathrm{e}^{AT})^{-1}(\xi J + \eta D), \qquad (18)\\ c(\eta) &\triangleq \mathrm{e}^{-(a_1+a_2+a_3)T}\left(1 + \eta\lambda CA(I - \mathrm{e}^{AT})^{-1}B\right). \qquad (19)\end{aligned}$$

Notice that the poles of $\psi(\cdot|\xi,\eta)$ are the real numbers $s = \mathrm{e}^{-a_i T}$, $i = 1,2,3$, according to (4). In the equations to follow, dependence on (ξ,η) in $\mathscr{Q}$ and ψ is dropped for brevity when it does not lead to confusion. Using the definitions of J and D in (14), it can be shown that $\psi(0|\eta,\xi)$ does not depend on ξ, since $C\,\mathrm{e}^{-AT}J = CB = 0$. Also, $c(\eta) = \psi(0|\xi,\eta)\,\mathrm{e}^{(a_1+a_2+a_3)T}$ for all pairs (ξ,η).

Theorem 2. *Let $\xi \le 0$ and $\eta \ge 0$ be arbitrary real constants.* ***Non-critical case:*** *If $c(\eta) \ne 0$, then $\mathscr{Q} = \mathscr{Q}(\xi,\eta)$ is Schur stable if and only if the three inequalities hold as follows:*

$$c(\eta) = \psi(0|\eta,\xi)\,\mathrm{e}^{(a_1+a_2+a_3)T} > -1, \tag{20}$$

$$\psi(-1) = 1 + C(I + \mathrm{e}^{AT})^{-1}(\xi J + \eta D) > 0, \tag{21}$$

$$c(\eta)\psi(c(\eta)|\xi,\eta) > 0. \tag{22}$$

In this case, the spectral radius of $\mathscr{Q}$ is greater than $|c(\eta)|$.

Critical case: *In the case where $c(\eta) = 0$, $\mathscr{Q}(\xi,\eta)$ is Schur stable if and only if (21) holds and*

$$|C\,\mathrm{e}^{-2AT}(\xi J + \eta D)| < \mathrm{e}^{(a_1+a_2+a_3)T}. \tag{23}$$

Proof. See Appendix C. □

Notice that the left-hand side of (22) is *linear* in ξ and rational in η. Hence, unlike the standard Schur stability conditions for matrices [15], [35], the conditions of Schur stability for Jacobian (14) prove to be *linear* in ξ. Similarly, (23) reduces to two inequalities that are linear in ξ.

The following corollary is straightforward by noticing that

$$Q'(X) = \mathscr{Q}(F'(\bar{y}_0), \Phi'(\bar{y}_0)),$$

Corollary 1. *The Jacobian (15) corresponding to a 1-cycle is Schur stable if and only if $\xi = F'(\bar{y}_0)$ and $\eta = \Phi'(\bar{y}_0)$ satisfy the stability conditions of Theorem 2.*

D. Local Convergence Rate

The eigenvalues of the Jacobian $Q'(X)$ (that is, the multipliers of the fixed point) define the convergence rate to the periodic solution and the dynamical character of the transients in vicinity of the fixed point. In dosing applications, to avoid overdosing, it is desirable to achieve monotone convergence to the steady-state conditions. With respect to (local) convergence to the desired 1-cycle, it is then required that the fixed point has to possess positive multipliers. The property can be demonstrated by diagonalizing the Jacobian by a state transformation since it describes the linearized dynamics of the discrete map $Q(\cdot)$ in (9).

By making use of (14), the problem of minimizing the spectral radius of the Jacobian by selecting K in (15) is

$$K^* = \arg\min_K \rho(A_\Phi + WKC),$$

where $\rho(\cdot)$ denotes the spectral radius. The problem of numerically minimizing the spectral radius of a nonsymmetric affine matrix function is considered in, e.g., [36]. It is both nonconvex and nonsmooth as the eigenvalues are generally not differentiable. Theorem 2 implies that the spectral radius cannot be reduced below $|c(\Phi'(\bar{y}_0)|$. Analyzing the definition (19), one notices that the factor $\mathrm{e}^{-(a_1+a_2+a_3)T} = \mathrm{e}^{-\alpha(v_1+v_2+v_3)T}$ is the larger, the smaller $\alpha > 0$ is. Therefore, patient models with smaller values of α will be more challenging to control to the desired periodic solution than those with higher values of the parameter. However, it can be shown (Corollary 3 in the Appendix) that $CA(I - \mathrm{e}^{AT})^{-1}B < 0$; thus, by choosing $\Phi'(\bar{y}_0) > 0$ large, one can decrease the value of $|c(\eta)|$ (and, as shown numerically below, as well the spectral radius).

a) Amplitude modulation: To obtain a better insight into the spectral properties of $Q'(\cdot)$ and how they depend on the impulsive controller, consider a special case of amplitude modulation that is obtained from (5) by letting $\Phi(z) \equiv T$. Then the Jacobian takes the form of

$$Q'_F(X) = A_\Phi + F'(\bar{y}_0)JC.$$

The stability condition (20) is automatically satisfied when $\eta = \Phi'(\bar{y}_0) = 0$. Furthermore, $c(0) = \mathrm{e}^{-(a_1+a_2+a_3)T}$ is usually very small for reasonable choices of T, for this reason,

$$\psi(c(0)|\xi,0) \approx \psi(0|\xi,0) = 1 - \xi C\,\mathrm{e}^{-TA}J = 1 - \xi CB = 1 > 0,$$

so that (22) typically holds unless $|F'(\bar{y}_0)|$ is very large. The most restrictive assumption is (21), which requires that

$$\frac{-1}{C(I + \mathrm{e}^{AT})^{-1}J} < \xi = F'(\bar{y}_0) < 0.$$

The coefficients of the characteristic polynomial (see Proposition 6 in the Appendix D) provide information on the eigenvalues $\lambda_1, \lambda_2, \lambda_3$, since $\gamma_1 = \mathrm{Tr}\; Q'_F(X) = \sum_i^3 \lambda_i$ and $\gamma_3 = \det Q'_F(X) = \prod_1^3 \lambda_i$. Apparently, the product of the eigenvalues of the Jacobian is independent of the amplitude modulation feedback, and a decrease in one of the eigenvalues will be accompanied with a rise in the other ones. The sum of the eigenvalues is an affine function of $F'(\bar{y}_0)$.

To maximize the convergence rate to the desired solution of the dynamics linearized at the fixed point of the closed-loop system (3), (5), one seeks the value of $F'(\bar{y}_0)$ that

minimizes the spectral radius of $Q'_F(X)$. Fig. 4 shows the absolute values of the eigenvalues of $Q'_F(X)$ as a function of $F'(\bar{y}_0)$. It is interesting that the spectral radius is minimized at the (Neimark-Sacker) bifurcation point where two eigenvalues of (40) become a complex conjugate pair. As shown in Appendix D, in this case the eigenvalues are found from the coefficients of the characteristic polynomial, so the spectral radius (conjectured to be minimal) can be found explicitly.

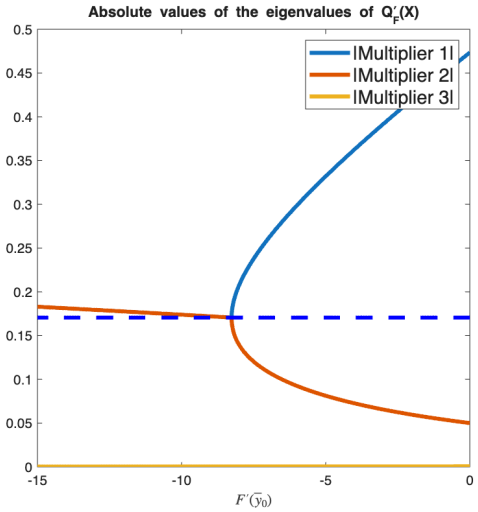


Fig. 4: Absolute values of the eigenvalues of $Q'_F(X)$ as function of $F'(\bar{y}_0)$. The minimal spectral radius is depicted by dashed line. The absolute values of two eigenvalues (a complex pair) coincide after the bifurcation point. The third eigenvalue (yellow line) is small in comparison with the other two and slowly decreases with the decreasing $F'(\bar{y}_0)$.

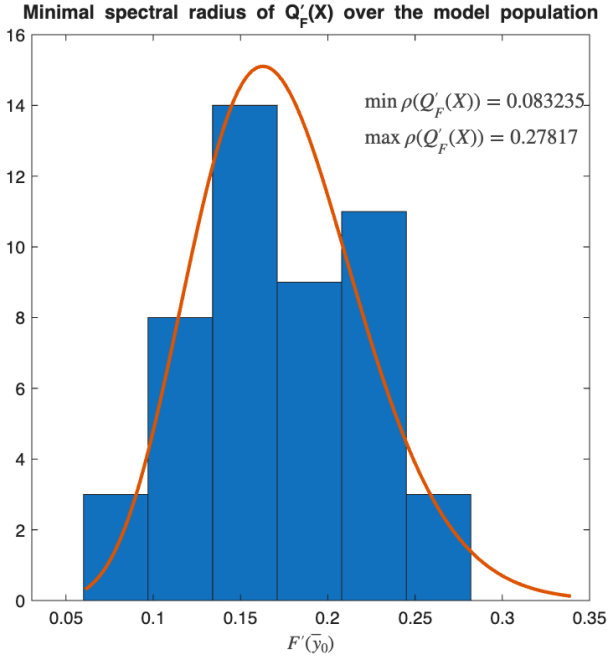


Fig. 5: Histogram of minimal spectral radii of $Q'_F(X)$ over the NMB model population. An approximation with a Beta distribution is provided for reference.

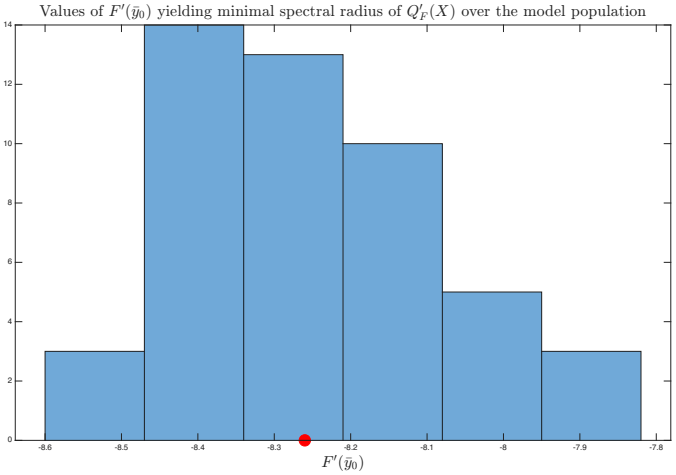


Fig. 6: Histogram of values of $F'(\bar{y}_0)$ yielding minimal spectral radius of $Q'_F(X)$ over the NMB model population. The optimal value for the population mean of $F'(\bar{y}_0) = -8.2600$ is marked with red circle.

The minimal spectral radius of $Q'_F(X)$ varies significantly over the considered model population, Fig. 5. Notably, this does not result in a wide spread of the optimal values of $F'(\bar{y}_0)$ at which the minimal spectral radius is achieved. The optimal value of $F'(\bar{y}_0)$ calculated for the population mean value of α appears approximately in the middle of the interval, see Fig. 5.

b) Phase modulation: Similarly to the case of pure amplitude modulation above, consider

$$Q'_\Phi(X) = \mathrm{e}^{AT} + \Phi'(\bar{y}_0)DC.$$

This type of impulsive feedback is obtained from (5) by assuming $F(\bar{y}_0) \equiv \lambda$. The slope of the frequency modulation function has to be positive in order to enforce sparser drug administration intervals for an elevated output. Taking into account the expression for D in (14), the Jacobian is found as

$$Q'_\Phi(X) = \mathrm{e}^{AT}\,(I - \mathrm{e}^{AT})^{-1}(I - \mathrm{e}^{AT} + \lambda\Phi'(\bar{y}_0)ABC).$$

Similar to the case of amplitude modulation, the fastest (local) convergence to the 1-cycle (i.e. the smallest spectral radius value of the Jacobian) is achieved by the impulsive feedback resulting in the Neimark-Sacker bifurcation, when complex values of the multipliers arise; see Fig. 7.

Over the model population, the achievable convergence rate values with respect to the frequency modulation feedback in Fig. 8 are distributed similarly to the case of amplitude modulation in Fig. 5. However, the required slopes of the frequency modulation characteristic are much lower; see Fig. 9. Once again, the value of $\Phi'(\bar{y}_0)$ corresponding to the population mean value of α is approximately in the middle of the range.

c) Amplitude and phase modulation: The convergence to the desired 1-cycle, when both amplitude and frequency modulation are exploited in the closed-loop system (3), (5), is difficult to analyze analytically. In Fig. 10, the spectral radius of $Q'(X)$ is calculated for the values of $\Phi'(\bar{y}_0)$ and $F'(\bar{y}_0)$ where the multipliers are real. For better visualization, spectral radius is assigned a value of minus one where there is a multiplier is complex. The manifolds where the direct and reverse

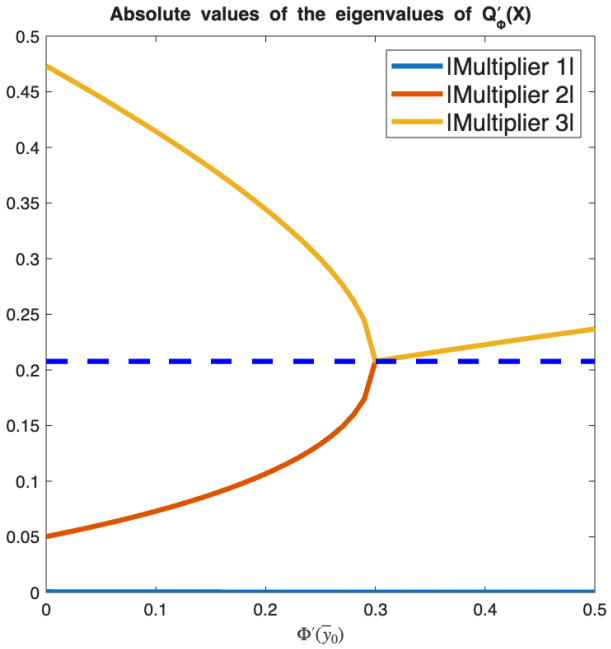


Fig. 7: Absolute values of the eigenvalues of $Q'_\Phi(X)$ as a function of $\Phi'(\bar{y}_0)$. The population mean value is assumed for α. The minimal spectral radius is depicted by a dashed line.

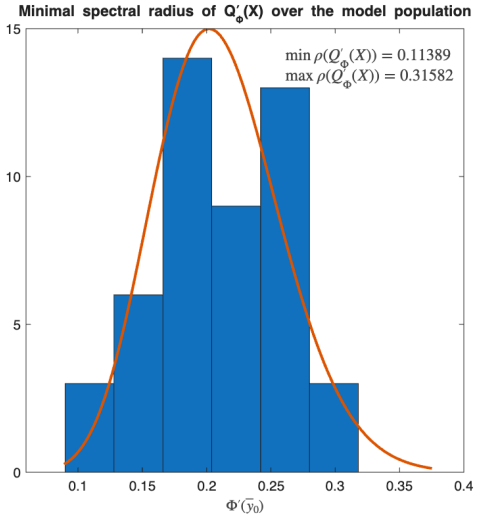


Fig. 8: Histogram of minimal spectral radii of $Q'_\Phi(X)$ over the NMB model population. An approximation with a Beta distribution is provided for reference.

Neimark-Sacker bifurcations occur (the edges in blue) seem to be affine functions of $\Phi'(\bar{y}_0)$ and $F'(\bar{y}_0)$. As seen before, the multipliers are always real for $\Phi'(\bar{y}_0) = F'(\bar{y}_0) = 0$. When $F'(\bar{y}_0)$ decreases from zero to some negative value, lower values of $\Phi'(\bar{y}_0)$ are required to preserve fixed point stability (cf. Theorem 2) and improve convergence without giving rise to oscillating transients. Soon, when $F'(\bar{y}_0) < -8.3$, the use of amplitude modulation definitely results in complex multipliers. This agrees well with what has been obtained for the case of purely amplitude modulation; cf. Fig. 6.

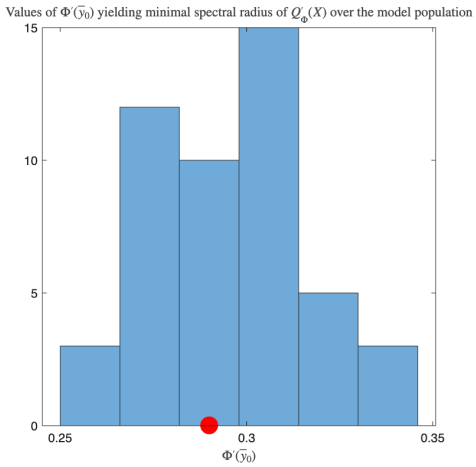


Fig. 9: Histogram of values of $\Phi'(\bar{y}_0)$ yielding minimal spectral radius of $Q'_\Phi(X)$ over the NMB model population. The optimal value for the population mean of $\Phi'(\bar{y}_0) = 0.29$ is marked with red circle.

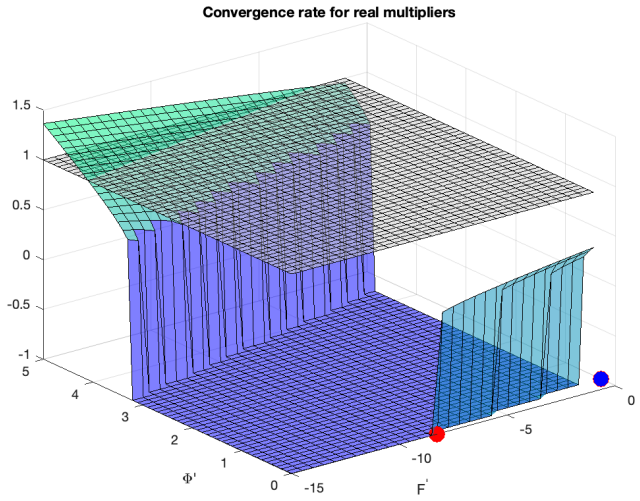


Fig. 10: Spectral radius of $Q'(X)$ as function of $\Phi'(\bar{y}_0)$ and $F'(\bar{y}_0)$. Green and light blue surfaces – spectral radius of the Jacobian when all the multipliers are real. Spectral radius is set to -1 when there are complex multipliers (dark blue area) for better visualization of bifurcation manifolds. Grey plane – stability border. Red circle – the optimal value $F'(\bar{y}_0) = -8.2600$ (only amplitude modulation) for the population mean α. Blue circle – the optimal value $\Phi'(\bar{y}_0) = 0.29$ (only frequency modulation) for the population mean α.

V. Impulsive Dosing Controller

Using *atracurium* in surgical practice, NMB is initiated with a bolus dose of 400–500 μg/kg. Further into the procedure, maintenance doses of 80–200 μg/kg are administered every 10–20 min. Under anesthesia, recovery to $y(t) = 25\%$ is achieved 35–45 min after injection, and recovery is usually 95% complete approximately one hour after injection. This is essentially an open-loop control strategy, but the medication effect is closely observed by means of an NMB monitor and

maintained within

$$\mathbf{y}_{\min} = 2 \leq y(t) \leq \mathbf{y}_{\max} = 10. \tag{24}$$

A. Open-loop administration

In Fig. 11, a scenario with a bolus dose of 400 μg/kg and a train of four sequential equidistant ($T = 20$ min) maintenance doses of 200 μg/kg is simulated for the model (1), (2) assuming the population mean values of the parameters, i.e. $\bar{\alpha}$, $\bar{\gamma}$. With a sustained maintenance phase ($T = 20$, $\lambda = 200$), the NMB effect converges to a 1-cycle corresponding to the fixed point

$$X^\top = [179.7316 \quad 56.3880 \quad 9.0833], \tag{25}$$

and yielding an output contained within the corridor $3.9866 \leq y(t) \leq 6.1562$, which satisfies (24). The corridor in which the periodic solution evolves can be computed without performing a simulation from Proposition 2 in [16]. The convergence to the 1-cycle is slow, and $\max_{t\in[T,5T]} y(t) = 5.6700$, thus revealing that the stationary solution is not reached. There is apparently also an overshoot of $\min y(t) = 2.6037$; that is, the system output goes under the lower bound of the corridor corresponding to the 1-cycle. Generally, the performance of the open-loop strategy for the population mean values of the parameters is acceptable since it complies with (24). Yet, across the considered population, the open-loop strategy fails to deliver the desired performance. The problems are particularly severe when it comes to the upper bound of the output corridor; see Fig. 13, where $\max_{t\in[T,5T]} y(t) \geq \mathbf{y}_{\max}$ is observed in 13 patient cases. In two cases, see Fig. 12, $\min_t y(t) > 10$ meaning that the output value is never under $\mathbf{y}_{\max}$.

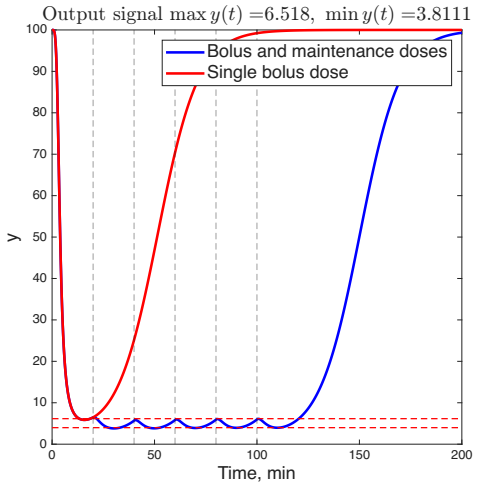


Fig. 11: Administration of *atracurium* in open loop. Population mean values are used in simulation. Response to a bolus dose of 400 μg/kg – solid red line. A bolus dose of 400 μg/kg followed by five maintenance doses each 20 min – blue line. Vertical dashed lines mark the instants of maintenance dose administration. The output corridor corresponding to a 1-cycle with $T = 20$ min and $\lambda = 200$ is depicted by dashed red lines.

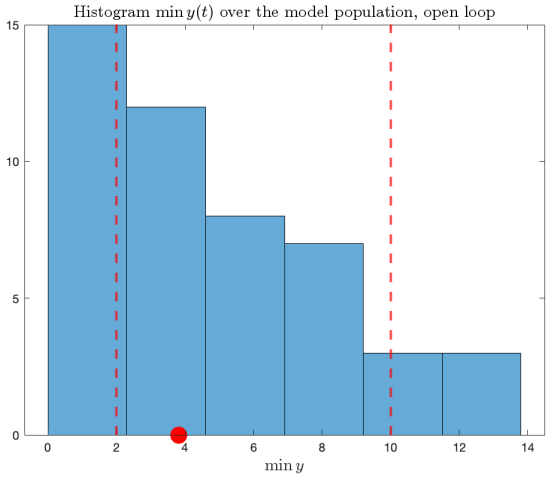


Fig. 12: Histogram of minimal values of $y(t)$ over the model population under open-loop administration. A bolus dose of 400 μg/kg followed by five maintenance doses 200 μg/kg each 20 min. Red circle shows the value achieved for population mean values. Desired interval of output values (24) is marked with red vertical dashed lines.

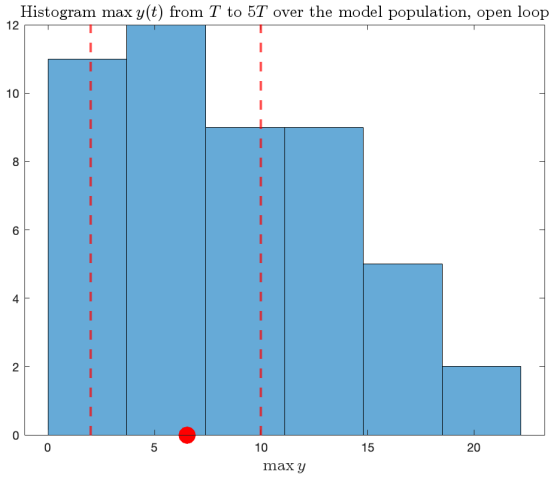


Fig. 13: Histogram of maximal values of $y(t)$ in the interval $[T, 5T]$ over the model population under open-loop administration. A bolus dose of 400 μg/kg followed by five maintenance doses 200 μg/kg each 20 min. Red circle shows the value achieved for population mean values. Desired interval of output values is marked with red vertical dashed lines.

B. Controller design algorithm

In view of the theoretical results presented above, the control problem formulated in Section III can be solved in the following way.

Step 1: Given the 1-cycle parameters λ and T, calculate the fixed point X by applying Theorem 1.

Step 2: Select suitable parametrizations of the modulation functions $\bar{F}(\cdot)$ and $\bar{\Phi}(\cdot)$.

Step 3: Pick up a point $\big(\bar{F}'(y_0), \bar{\Phi}'(y_0)\big)$ satisfying the stability condition of 1-cycle from Theorem 2.

Step 4: For the selected in Step 2 parametrizations, solve the equations

$$\frac{\mathrm{d}}{\mathrm{d}\theta}\bar{F}(\theta)|_{\theta=y_0} = \bar{F}'(y_0), \quad \frac{\mathrm{d}}{\mathrm{d}\theta}\bar{\Phi}(\theta)|_{\theta=y_0} = \bar{\Phi}'(y_0)$$

with respect to the parameters defining the slopes of the modulation functions.

Step 5: Solve the equations

$$F(\bar{y}_0) = \lambda, \quad \Phi(\bar{y}_0) = T,$$

with respect to the parameters of $\bar{F}(\cdot), \bar{\Phi}(\cdot)$.

Recall that the choice of the slopes of the modulation functions in Step 3 influences, besides stability of the periodic solution, the transient properties of the closed-loop system when converging to the 1-cycle from an initial condition outside of it.

C. Implementation

The pulse-modulated controller design procedure specified above is applied in this section to the NMB model in (1), (2) assuming the population mean values of the parameters.

Step 1: The fixed point corresponding to the 1-cycle parameters $\lambda = 200$, $T = 20$ is given by (25).

Step 2: Following [16], select $\bar{F}(\cdot), \bar{\Phi}(\cdot)$ in (7) as piecewise affine, i.e.

$$\bar{\Phi}(\xi) = \begin{cases} \Phi_2 & \Phi_2 < k_2\xi + k_1, \\ k_2\xi + k_1 & \Phi_1 \le k_2\xi + k_1 \le \Phi_2, \\ \Phi_1 & k_2\xi + k_1 < \Phi_1, \end{cases} \tag{26}$$

$$\bar{F}(\xi) = \begin{cases} F_1 & k_4\xi + k_3 < F_1, \\ k_4\xi + k_3 & F_1 \le k_4\xi + k_3 \le F_2, \\ F_2 & F_2 < k_4\xi + k_3. \end{cases} \tag{27}$$

Recalling from (2) that $y(t) \in [0, 100]$, the following inequalities apply

$$\Phi_1 \le k_1,\ 100k_2{+}k_1 \le \Phi_2,\ F_1 \le k_3,\ 100k_4{+}k_3 \le F_2. \tag{28}$$

From the bounds on the modulation functions, it follows that the feedback cannot administer a dose that is greater than F_2 or less than F_1. Further, no dose is administered sooner than Φ_1 from the previous one and at least one dose is administered within a time interval of Φ_2. Numerical values of these bounds can be easily obtained from the manual medication protocols for the drug in question.

The affine form of the modulation functions results in linear design equations but has an apparent limitation. The functions $\bar{F}(\cdot)$ and $\bar{\Phi}(\cdot)$ are completely defined by the fixed point X (i.e. the values of λ, T) and the slopes k_4, k_2 calculated in *Step 4* to guarantee stability. If an additional dosing condition has to be satisfied, e.g. a certain bolus dose has to be administered in the beginning of the surgery ($\bar{F}(100\%)$), than a compromise has to be made or a more accommodating parametrerization of the modulation functions selected.

Step 3: Choose the slopes of the modulation functions at the fixed point as $F'(y_0) = -2$ and $\Phi'(y_0) = 0.7$. For stability condition (20), it applies

$$0.8156 > -1.2825 \cdot 10^9.$$

Stability condition (21) then reads

$$0.0454 \cdot F'(\bar{y}_0) - 0.5700 \cdot \Phi'(\bar{y}_0) = -0.4898 > -1.$$

Condition (22) gives

$$5.1721 \cdot 10^{-10} > 0$$

and orbital stability of the periodic solution is therefore guaranteed according to Theorem 2. The spectral radius of the Jacobian $\rho(Q'(X)) = 0.2349$ and the eigenvalue spectrum $\sigma(Q'(X)) = \{0.1551 \pm 0.1765i,\ 0.0002\}$.

Step 4: For $F'(\cdot)$ and $\Phi'(\cdot)$ in (27),(26), by applying the chain rule

$$\begin{aligned} F'(\bar{y}_0) &= \bar{F}'(\bar{y}_0)\varphi'(\bar{y}_0) = k_4\varphi'(\bar{y}_0), \\ \Phi'(\bar{y}_0) &= \bar{\Phi}'(\bar{y}_0)\varphi'(\bar{y}_0) = k_2\varphi'(\bar{y}_0), \end{aligned} \tag{29}$$

where $\bar{y}_0 = CX$ and

$$\varphi'(\xi) = -\frac{\gamma 100 C_{50}^{\gamma} \xi^{\gamma-1}}{\left(C_{50}^{\gamma} + \xi^{\gamma}\right)^2}.$$

This yields the numerical values $\bar{y}_0 = 9.0833$, $\varphi'(\bar{y}_0) = -1.6616$, $k_4 = 1.2036$, $k_2 = -0.4213$.

Step 5: To obtain a 1-cycle with the desired parameters, the following equations have to hold

$$\begin{aligned} F(\bar{y}_0) &= (\bar{F} \circ \varphi)(\bar{y}_0) = k_4\varphi(\bar{y}_0) + k_3 = \lambda, \\ \Phi(\bar{y}_0) &= (\bar{\Phi} \circ \varphi)(\bar{y}_0) = k_2\varphi(\bar{y}_0) + k_1 = T, \end{aligned} \tag{30}$$

thus yielding $k_3 = 192.7539$, $k_1 = 22.5361$.

Now the pulse-modulated feedback controller is designed and the resulting modulation functions are depicted in Fig. 14.

D. Feedback controller evaluation

Consider the same 1-cycle as obtained in the open-loop administration (Section V-A), i.e. the one defined by the fixed point in (25), but implemented in closed-loop system (1), (2), (5). A periodic solution of the closed-loop system corresponding to this fixed point is shown in Fig. 15.

A feedback drug administration system is expected to work in a wide range of the plant output values. Transient behaviors to the designed periodic solution from a distant point in the state space are therefore important. An underdosing of an NMB agent, i.e. $\exists\ t : \mathbf{y}_{\max} < y(t)$, is more critical than an overdosing event, i.e. $\exists\ t : y(t) < \mathbf{y}_{\min}$, since there is a risk of disrupting the surgery in the former case. For the design case considered in Section V-C, the transient process corresponding to a start of a surgical procedure, i.e. $x(0) = 0,\ y(0) = 100\%$, is shown in Fig. 16. The controller satisfies the clinical output range in (24) but exhibits an overshoot with respect to the bounds of the 1-cycle resulting from the complex eigenvalues of the Jacobian, cf. Step 3 in Section V-C. This can be addressed by reducing the slope of the frequency modulation function to the value corresponding to the Neimark-Sacker bifurcation, cf. (41), and maximizing the (local) convergence

rate. Then, the overshoot is reduced from $\inf_t y(t) = 2.9689$ to $\inf_t y(t) = 3.2252$, i.e. from 25.5% to 19% with respect to lower output corridor bound. This is in fact worse compared to open-loop administration in Fig. 11, where the overshoot is only 4.4%. Yet, in open loop, there is an undershoot that is not at all present in closed-loop administration. Notice that the performance of the pulse-modulated controller can be further tuned for a particular combination of (α, γ) but is not performed here as the clinical output range in (24) is well satisfied.

To study the performance of the pulse-modulated NMB agent controller across the patient model population, four design cases resulting in different modulation functions are now considered, see Table I. Open-loop administration is denoted as Case 0. The evaluation criteria are the incidence of NMB agent underdosing and overdosing defined according to (24). Histograms of the minimal and maximal values of the PK/PD plant output for the different design cases are provided in Fig. 19 and Fig. 18, correspondingly. Notice that the maximal value of is calculated over the interval $t \in [T, 5T]$ since it always holds that $\sup_t y(t) = y(0) = 100\%$.

By inspection of the histograms, it can be concluded that the introduction of the feedback has major impact on the underdosing events but not on the overdosing ones. Actually, pulse-modulated feedback either performs similar to the open-loop administration (or even worse) since the first dose is always provided at $t = 0$ and is equal to the bolus dose according to the evaluation protocol. A straightforward way of handling this issue is to start with lower bolus doses and allow the feedback to activate earlier (i.e. use a lower Φ_1). This will of course prolong the induction phase of NMB. Applying the open-loop administration (Case 0), underdosing is observed at 18 instances across the cohort (Table I), which is reduced to 11 instances under feedback (Case 2). In Case 1, the highest values of the output are nicely grouping at that of the population mean values. It is also the only design case where the lowest values of the output are never over the bound $\mathbf{y}_{\max}$. In contrast, the open-loop administration yields four cases where the output $y(t)$ lies over the bound $\mathbf{y}_{\max}$ all the time, i.e. $\forall t : \mathbf{y}_{\max} < y(t)$.

The robustness properties of the proposed pulse-modulated controller are illustrated in Fig. 20. As expected, controlling models with very high or very low values of γ with the same controller presents significant challenges. Low values of γ lead to underdosing and high values of γ result in overdosing. Combinations of low α and extreme values of γ are especially difficult to deal with and always exhibit over- or underdosing under an impulsive feedback designed for the population mean values. Recall that the open-loop strategy fails to maintain clinical NMB interval (24) in two thirds of the modeled cases (i.e. 32 out of 48, see Tab. I).

VI. Conclusions

A pulse-modulated feedback controller employing both amplitude and frequency modulation is considered. The closed-loop dynamics of the controller governing a continuous time-invariant single-input single-output nonlinear plant of Wiener structure are captured by a discrete map. A controller design procedure to produce a sustained stationary periodic solution with given parameters is proposed. It is based on calculating the fixed point of the discrete map corresponding to the desired periodic solution and stabilizing it by choosing the slopes of the modulation functions. A necessary and sufficient stability condition for a periodic solution with only one firing of the feedback in the least period is proven. The utility of the proposed controller is illustrated by a dosing application of a neuro-muscular blockade agent widely applied in anesthesiology. A simulation study on a database of pharmacokinetic-pharmacodynamic models estimated from clinical data shows a significant improvement in the incidence of underdosing events compared to an open-loop administration scheme. To reduce the incidence of overdosing events in the induction phase, a high bolus dose has to be substituted by a sequence of lower doses which would result in a prolonged NMB induction phase.

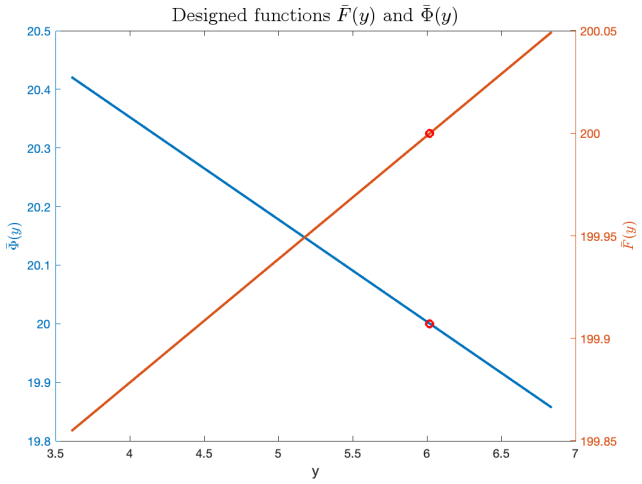


Fig. 14: The affine parts of the designed functions $\bar{F}(\cdot)$, $\bar{\Phi}(\cdot)$. The values $\bar{F}(y_0)$, $\bar{\Phi}(y_0)$ are marked with red circle.

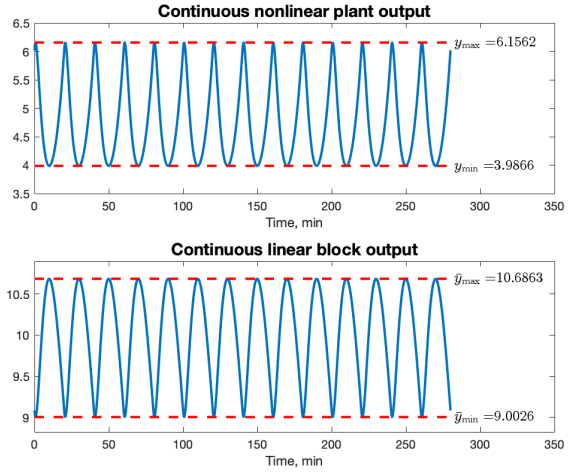


Fig. 15: The designed 1-cycle initiated from the fixed point X. The nonlinear output $y(t)$ (top plot) and the linear output $\bar{y}(t)$ (bottom plot) are presented.

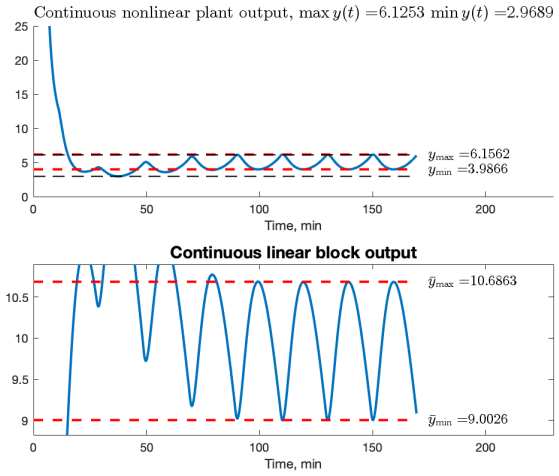


Fig. 16: The transient process from $x(0) = 0,\ y(0) = 100\%$ to the designed 1-cycle for $F'(y_0) = -2,\ \Phi'(y_0) = 0.7$, Case 2 in Table I. The nonlinear output $y(t)$ (top plot) and the linear output $\bar{y}(t)$ (bottom plot) are presented. The horizontal red dashed lines show the output corridor bounds for the nonlinear/linear output. The horizontal black dashed lines mark $\inf_t y(t)$ and $\sup_{t\in[T,5T]} y(t)$.

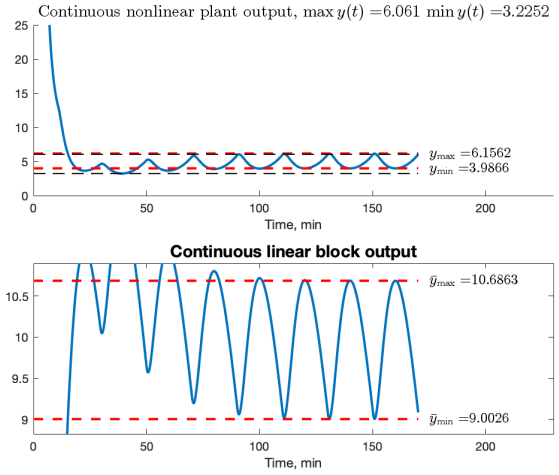
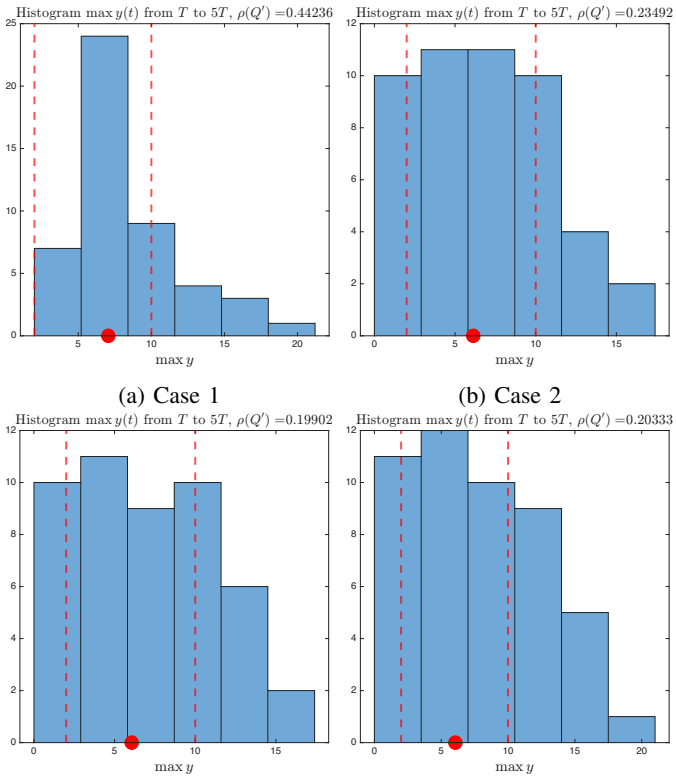


Fig. 17: The transient process from $x(0) = 0,\ y(0) = 100\%$ to the designed 1-cycle for $F'(y_0) = -2,\ \Phi'(y_0) = 0.33707$ (Neimark-Sacker bifurcation point), Case 3 in Table I. The nonlinear output $y(t)$ (top plot) and the linear output $\bar{y}(t)$ (bottom plot) are presented. The horizontal red dashed lines show the output corridor bounds for the nonlinear/linear output. The horizontal black dash lines mark $\inf_t y(t)$ and $\sup_{t\in[T,5T]} y(t)$.



(a) Case 1 (b) Case 2

(c) Case 3 (d) Case 4

Fig. 18: Histograms of $\sup_{t\in[T,5T]} y(t)$ across the patient cohort for the design cases in Table. I. The vertical dashed lines correspond to $\mathbf{y}_{\min}$, $\mathbf{y}_{\max}$ in (24).

	$F';\Phi'$	$\rho(Q')$	PIN, $y < \mathbf{y}_{\min}$	PIN, $y > \mathbf{y}_{\max}$
Case 0	0; 0	0.4829	1,7,16,17,21,27, 28,29,32,33,36, 40,41,48	2,4,6,9,10,11,12, 15,22,24,25,26,37, 39,43,44,45,46
Case 1	-1; 4	0.4424	1,7,13,14,16,17, 19,21,27,28,29, 32,33,36,40,41,48	4,6,11,12,15,22,24, 25,26,37,43,46
Case 2	-2; 0.7	0.2349	1,7,16,17,21,27, 28,29,32,33,36,40, 41,48	2,6,11,24,25,26,37, 39,43,44,46
Case 3	-2; 0.337	0.1990	1,7,16,17,21,27, 28,29,32,33,36, 40,41,48	2,6,9,11,12,24,25, 26,37,39,43,44,46
Case 4	-1; 0.392	0.2033	1,7,16,17,21,27, 28,29,32,33,36, 40,41,48	2,4,6,9,11,12,15, 22,24,25,26,37,39, 43,44,46

TABLE I: Pulse-modulated controller design cases

REFERENCES

[1] A. Albassam and D. A. Hughes, "What should patients do if they miss a dose? a systematic review of patient information leaflets and summaries of product characteristics," *European journal of clinical pharmacology*, vol. 77, no. 2, pp. 251–260, 2021.

[2] A. K. Gelig and A. N. Churilov, *Stability and Oscillations of Nonlinear Pulse-modulated Systems*. Boston: Birkhäuser, 1998.

[3] V. Lakshmikantham, D. D. Bainov, and P. S. Simeonov, *Theory of Impulsive Differential Equations*. Singapore: World Scientific, 1989.

[4] A. M. Samoilenko and N. A. Perestyuk, *Impulsive Differential Equations*. Singapore: World Scientific, 1995.

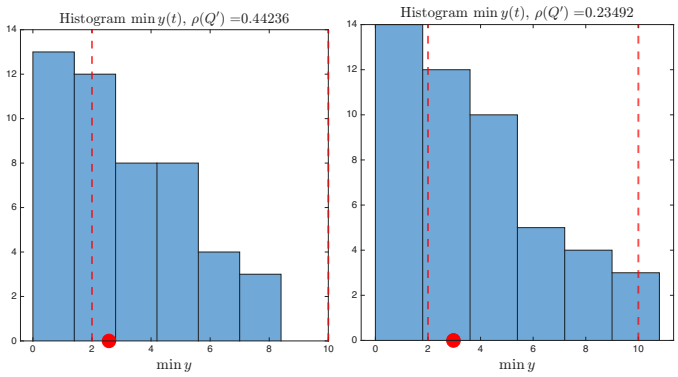
[5] J. Walker, J. R. Terry, K. Tsaneva-Atanasova, S. Armstrong, C. McArdle, and S. L. Lightman, "Encoding and decoding mechanisms of pulsatile hormone secretion," *J Neuroendocrinol.*, vol. 22, no. 12, pp. 1226–1238, December 2010.

[6] A. Medvedev, A. V. Proskurnikov, and Z. T. Zhusubaliyev, "Mathematical modeling of endocrine regulation subject to circadian rhythm," *Annual Reviews in Control*, vol. 46, pp. 148–164, 2018.

[7] H. Taghvafard, A. Medvedev, A. V. Proskurnikov, and M. Cao, "Impulsive model of endocrine regulation with a local continuous feedback," *Math Biosci.*, no. 310, pp. 128–135, 2019.

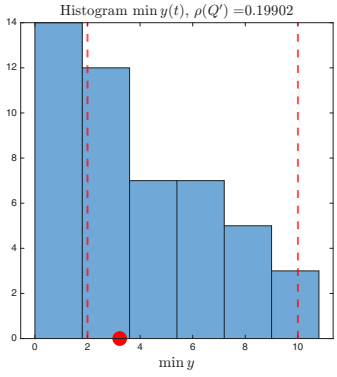
[8] J. Alford and G. Hida, "Discrete systems in process control," *AIChE CEP magazine*, pp. 57–63, June 2022.

[9] R. Bellman, "Topics in pharmacokinetics, iii: Repeated dosage and impulse control," *Mathematical Biosciences*, vol. 12, no. 1, pp. 1–5,

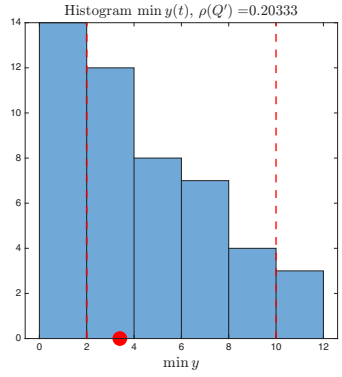


(a) Case 1

(b) Case 2



(c) Case 3



(d) Case 4

Fig. 19: Histograms of $\inf_t y(t)$ across the patient cohort for the design cases in Table I. The vertical dashed lines correspond to $\mathbf{y}_{\min}$, $\mathbf{y}_{\max}$ in (24).

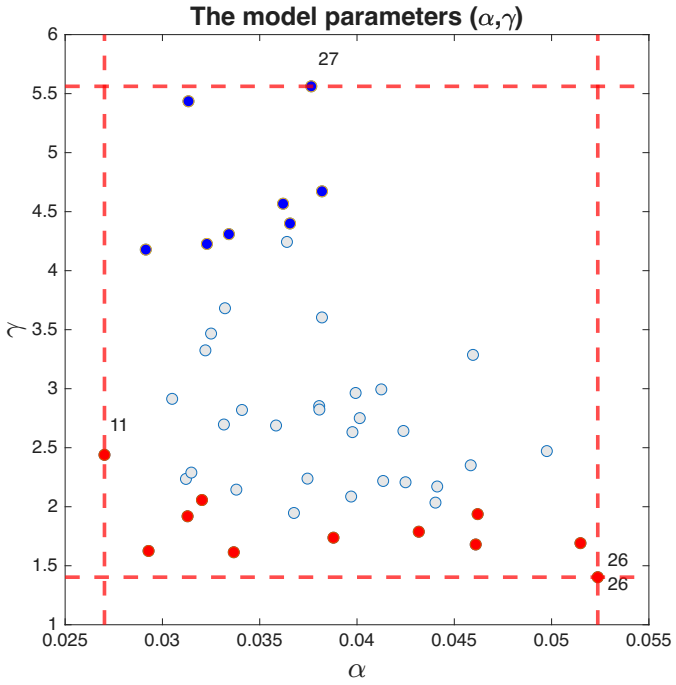


Fig. 20: The model parameter pairs in the data set. The controller design in Case 2 is applied. Underdosing ($\sup_{t\in[T,5T]} y(t) < \mathbf{y}_{\max}$) – red dots. Overdosing ($\inf_t y(t) > \mathbf{y}_{\min}$) – blue dots. The extreme parameter values are indicated by the Patient Identification Number.

1971.

[10] P. Sopasakis, P. Patrinos, H. Sarimveis, and A. Bemporad, "Model predictive control for linear impulsive systems," *IEEE Transactions on Automatic Control*, vol. 60, no. 8, pp. 2277–2282, 2015.

[11] P. S. Rivadeneira, J. Godoy, J. Sereno, P. Abuin, A. Ferramosca, and A. González, "Impulsive MPC schemes for biomedical processes: Application to type 1 diabetes," in *Control Applications for Biomedical Engineering Systems*, A. T. Azar, Ed. Academic Press, 2020, pp. 55–87.

[12] E. Estremera, A. Beneyto, A. Cabrera, I. Contreras, and J. Vehí, "Intermittent closed-loop blood glucose control for people with type 1 diabetes on multiple daily injections," *Computer Methods and Programs in Biomedicine*, vol. 236, p. 107568, 2023.

[13] K. Polonsky, B. D. Given, and E. Van Cauter, "Twenty-four-hour profiles and pulsatile patterns of insulin secretion in normal and obese subjects," *J Clin Invest.*, vol. 81, pp. 442–448, February 1988.

[14] A. Medvedev, A. V. Proskurnikov, and Z. T. Zhusubaliyev, "Design of the impulsive Goodwin's oscillator: A case study," in *American Control Conference*, San Diego, CA, 2023.

[15] ——, "Design of the impulsive Goodwin's oscillator in 1-cycle," *IFAC-PapersOnLine*, vol. 56, no. 2, pp. 6660–6665, 2023, Proceedings of the 22nd IFAC World Congress.

[16] ——, "Output corridor control via design of impulsive Goodwin's oscillator," in *American Control Conference*, Toronto, Canada, 2024.

[17] A. Medvedev, A. Churilov, and A. Shepeljavyi, "Mathematical models of testosterone regulation," in *Stochastic optimization in informatics*. Saint Petersburg State University, 2006, no. 2, pp. 147–158, in Russian.

[18] A. Churilov, A. Medvedev, and A. Shepeljavyi, "Mathematical model of non-basal testosterone regulation in the male by pulse modulated feedback," *Automatica*, vol. 45, no. 1, pp. 78–85, 2009.

[19] A. V. Proskurnikov, H. Runvik, and A. Medvedev, "Cycles in impulsive Goodwin's oscillators of arbitrary order," *Automatica*, vol. 159, January 2024, article 111379.

[20] C. D. McGrath and J. M. Hunter, "Monitoring of neuromuscular block," *Continuing Education in Anaesthesia Critical Care & Pain*, vol. 6, no. 1, pp. 7–12, 02 2006.

[21] M. L. Thompson Bastin, R. R. Smith, B. D. Bissell, H. N. Wolf, A. M. Wiegand, M. E. Cavagnini, Y. Ahmad, and A. H. Flannery, "Comparison of fixed dose versus train-of-four titration of cisatracurium in acute respiratory distress syndrome," *Journal of Critical Care*, vol. 65, pp. 86–90, 2021.

[22] V. Tsolaki, G. Zakynthinos, M. Papadonta, F. Bardaka, G. Fotakopoulos, I. Pantazopoulos, D. Makris, and E. Zakynthinos, "Neuromuscular blockade in the pre- and COVID-19 ARDS patients," *J Pers Med.*, vol. 12, no. 9, p. 1538, 2022.

[23] C. M. Wait, V. A. Goat, and C. E. Blogg, "Feedback control of neuromuscular blockade," *Anaesthesia*, vol. 42, no. 11, pp. 1212–1217, 1987.

[24] P. C. Uys, D. F. Morrell, H. S. Bradlow, and L. B. Rametti, "Self-tuning, microprocessor-based closed-loop control of atracurium-induced neuromuscular blockade," *Br J Anaesth.*, vol. 61, no. 6, pp. 685–692, 1988.

[25] Z. T. Zhusubaliyev, A. Medvedev, and M. Silva, "Bifurcation analysis of PID controlled neuromuscular blockade in closed-loop anesthesia," *Journal of Process Control*, vol. 25, pp. 152 – 163, January 2015.

[26] A. Medvedev, Z. T. Zhusubaliyev, O. Rosén, and M. M. Silva, "Oscillations-free PID control of anesthetic drug delivery in neuromuscular blockade," *Computer Methods and Programs in Biomedicine*, vol. 171, pp. 119–131, 2019.

[27] M. M. da Silva, T. Wigren, and T. Mendonca, "Nonlinear identification of a minimal neuromuscular blockade model in anesthesia," *IEEE Transactions on Control Systems Technology*, vol. 20, no. 1, pp. 181–188, 2012.

[28] O. Rosén, M. Silva, and A. Medvedev, "Nonlinear estimation of a parsimonious Wiener model for the neuromuscular blockade in closed-loop anesthesia," in *19th World Congress, The International Federation of Automatic Control*, Cape Town, South Africa, 2014.

[29] A. Medvedev, Z. T. Zhusubaliyev, O. Rosén, and M. Silva, "Oscillations-free PID control of anesthetic drug delivery in neuromuscular blockade," *Computer Methods and Programs in Biomedicine*, July 2016.

[30] Z. T. Zhusubaliyev, A. Churilov, and A. Medvedev, "Bifurcation phenomena in an impulsive model of non-basal testosterone regulation," *Chaos*, vol. 22, no. 1, p. 013121, 2012.

[31] Z. T. Zhusubaliyev and E. Mosekilde, *Bifurcations and Chaos in Piecewise-Smooth Dynamical Systems*. World Scientific, 2003.

[32] J. Eller, "On functions of companion matrices," *Linear Algebra and its Applications*, vol. 96, pp. 191–210, 1987.
[33] C. de Boor, "Divided differences," *Surveys in Approximation Theory*, vol. 1, pp. 46–69, 2005.
[34] Y.-Y. Cao, J. Lam, and Y.-X. Sun, "Static output feedback stabilization: An ILMI approach," *Automatica*, vol. 34, no. 12, pp. 1641–1645, 1998.
[35] R. Fleming, G. Grossman, T. Lenker, S. Narayan, and S.-C. Ong, "On schur d-stable matrices," *Linear Algebra and its Applications*, vol. 279, pp. 39–50, 1998.
[36] M. L. Overton and R. S. Womersley, "On minimizing the special radius of a nonsymmetric matrix function: Optimality conditions and duality theory," *SIAM Journal on Matrix Analysis and Applications*, vol. 9, no. 4, pp. 473–498, 1988.

APPENDIX A
THE OPITZ FORMULA FOR 3×3 MATRICES

Given a function f, which is complex-analytic in a vicinity of the spectrum $\{-a_1, -a_2, -a_3\}$ of the matrix A from (3), the Opitz formula [19], [33] states that

$$f(A) = \begin{bmatrix} f(-a_1) & 0 & 0 \\ g_1 f[-a_1, -a_2] & f(-a_2) & 0 \\ g_1 g_2 f[-a_1, -a_2, -a_3] & g_2 f[-a_2, -a_3] & f(-a_3) \end{bmatrix}.$$

Whereas the Opitz formula is valid for two-diagonal matrices of arbitrary dimensions [33], the three-dimensional case can be proved in a straightforward manner through reducing A and $f(A)$ to the diagonal forms. Introducing the matrices

$$S = \begin{bmatrix} 1 & 0 & 0 \\ \frac{g_1}{a_2 - a_1} & 1 & 0 \\ \frac{g_1 g_2}{(a_2 - a_1)(a_3 - a_1)} & \frac{g_2}{a_3 - a_2} & 1 \end{bmatrix} \tag{31}$$

$$S^{-1} = \begin{bmatrix} 1 & 0 & 0 \\ \frac{g_1}{a_1 - a_2} & 1 & 0 \\ \frac{g_1 g_2}{(a_1 - a_3)(a_2 - a_3)} & \frac{g_2}{a_2 - a_3} & 1 \end{bmatrix}, \tag{32}$$

a straightforward computation shows that

$$A = S \begin{bmatrix} -a_1 & 0 & 0 \\ 0 & -a_2 & 0 \\ 0 & 0 & -a_3 \end{bmatrix} S^{-1}, \tag{33}$$

$$f(A) = S \begin{bmatrix} f(-a_1) & 0 & 0 \\ 0 & f(-a_2) & 0 \\ 0 & 0 & f(-a_3) \end{bmatrix} S^{-1}. \tag{34}$$

Equations (31)-(34) will be used in the proof of Theorem 2.

An important property of the divided differences is the generalized mean-value formula [33]. Assuming, without loss of generality, that $x_0 < x_1 < x_2$, one has

$$\begin{aligned} f[x_0, x_1] &= f'(\bar{\theta}) \quad \text{for some } \bar{\theta} \in [x_0, x_1], \\ f[x_0, x_1, x_2] &= \frac{1}{2} f''(\tilde{\theta}) \quad \text{for some } \tilde{\theta} \in [x_0, x_2]. \end{aligned} \tag{35}$$

This entails the following simple yet important proposition.

Proposition 1. *Let function $f : (-\infty, 0) \to \mathbb{R}$ be strictly convex and $T > 0$. Then, $Cf(TA)B > 0$. If, additionally, f is increasing and positive, then the vector $f(TA)B$ is positive.*

Proof: The proof is straightforward by applying the Opitz formula and (35) to the matrix TA with the eigenvalues $(-Ta_i) < 0$ and noticing that $Cf(TA)B$ is nothing else than the $(3,1)$ entry of $f(TA)$ and $f(TA)B$ is its first column. ■

Corollary 2. *For $\mu(x) = 1/(\mathrm{e}^{-x} - 1)$ and $\nu(x) = -x\mu(x)$, the vectors $\mu(TA)B$ and $\nu(TA)B$ are positive.*

Proof: Obviously, the function $\mu(x) = 1/(\mathrm{e}^{-x} - 1)$ restricted to the interval $x \in (-\infty, 0)$ is positive and increasing. After some computation, one checks that

$$\mu''(x) = \frac{e^{-x}(1 + e^{-x})}{(e^{-x} - 1)^3} > 0 \quad \forall x < 0,$$

in other words, μ is convex on $(-\infty, 0)$. The first statement is now immediate from Proposition 1.

Similarly, $\nu(x) > 0$ for $x < 0$. To prove the monotonicity and convexity, note first that $1 - (x+1)\,\mathrm{e}^{-x}$ is strict decreasing on $(-\infty, 0]$ and thus achieves its minimum (0) at $x = 0$. Therefore, ν is strict increasing on $(-\infty, 0]$ as

$$\nu'(x) = \frac{1 - (x+1)\,\mathrm{e}^{-x}}{(1 - \mathrm{e}^{-x})^2} > 0 \quad \forall x < 0.$$

Finally, a direct yet tedious computation shows that

$$\nu''(x) = -\,\mathrm{e}^{-x}\,\frac{((2+x)\,\mathrm{e}^{-x} + x - 2)}{(\mathrm{e}^{-x} - 1)^3},$$

where the numerator is negative for $x < 0$ as

$$\frac{d}{dx}\left((2+x)\,\mathrm{e}^{-x} + x - 2\right) = 1 - (1+x)\,\mathrm{e}^{-x} > 0 \quad \forall x < 0.$$

Hence, the function $(2 + x)\,\mathrm{e}^{-x} + x - 2$ is increasing on $(-\infty, 0)$ and achieves its strict maximum (0) at $x = 0$. This proves the strict convexity $\nu''(x) > 0 \ \ \forall x < 0$. ■

Corollary 3. *For $\varrho(x) = x/(1 - \mathrm{e}^{x})$, the number $C\varrho(\mathrm{e}^{TA})B$ is negative for all $T > 0$.*

Proof: Similar to the previous corollary, one obtains

$$\varrho''(x) = \frac{\mathrm{e}^{x}}{(1 - \mathrm{e}^{x})^3}\,(x + 2 + x\,\mathrm{e}^{x} - 2\,\mathrm{e}^{x}),$$

As we know from the previous proof, $(x+2)\,\mathrm{e}^{-x} + x - 2 < 0$ when $x < 0$, and therefore ρ is strict concave. ■

APPENDIX B
PROOFS OF THEOREM 1 AND LEMMA 1

Applying the Opitz formula (Appendix A) to the matrix TA, where A is defined as in (3), $T > 0$, and $f \equiv \mu$, one easily checks that (12) can be equivalently rewritten[2] as

$$X = \lambda\mu(TA)B = \lambda(e^{-AT} - I)^{-1}B,$$

which, in turn, is equivalent to the relation

$$X = \mathrm{e}^{TA}(X + \lambda B). \tag{36}$$

In view of Corollary 2, the vector X from (12) is positive.

Proof of Theorem 1

To prove the implication 2) $\Longrightarrow$ 1), recall that 1-cycle with the impulse weight $\lambda_n \equiv \lambda$ and the pulse width $t_{n+1} - t_n \equiv T$ corresponds to the fixed point $X(t_n^-) \equiv X$ of Q whose output $\bar{y}_0 = CX$ satisfies (13). Substituting $X_n = X_{n+1} = X$ and (13) into (9), one proves (36), which is equivalent to (12).

The proof of implication 1) $\Longrightarrow$ 2) is similar: Since (12) and (13) (where $\bar{y}_0 = CX$) imply (36), the vector X from (12) is a fixed point of Q. Furthermore, (13) implies that X corresponds to a 1-cycle with parameters λ, T. ■

[2]The inverse matrix is well-defined since the eigenvalues e^{Ta_i} of e^{-TA} are, obviously, greater than 1.

Proof of Lemma 1

The proof follows from the definition of vectors D, J and the Opitz formula (Appendix A).

The vector J, being the first column of the matrix $\mathrm{e}^{A\Phi(z_0)}$, is strictly positive in view of Proposition 1 as the function $x \mapsto \mathrm{e}^x$ is monotone increasing and convex on the real line.

In order to prove that $D = AX < 0$, notice that

$$D = A(\mathrm{e}^{-A\Phi(z_0)} - I)^{-1}B = -T^{-1}\nu(TA)B,$$

where $\nu(z) = -z\mu(z) = \frac{z}{1-\mathrm{e}^{-z}}$. The statement is now immediate from Corollary 2. ∎

Appendix C
Proof of Theorem 2

First, some technical properties for the functions χ, ψ defined in (37) and (18) are established. Also, unless otherwise stated, $\xi \le 0$ and $\eta \ge 0$ assumed. Recall that, in view of (4), one has $a_1 < a_2 < a_3$.

Along with the functions (18) and (19), we will use the characteristic polynomial of $\mathscr{Q}$, that is,

$$\chi(s|\xi,\eta) \triangleq \det\left(sI - \mathscr{Q}(\xi,\eta)\right). \tag{37}$$

Technical propositions

Proposition 2. *The functions $\psi(s|\xi,\eta)$ and $\chi(s|\xi,\eta)$ have no zeros in the interval $s \in (\mathrm{e}^{-a_1T}, \infty)$. In particular, all* real positive *eigenvalues of matrix $\mathscr{Q}$, if they exist, are stable.*

Proof: Retracing the proof of Lemma 1, recall that $J > 0$ and $D < 0$, therefore, $\xi J \le 0$ and $\eta D \le 0$. By the model construction (i.e. (4)), a_1 is the minimal eigenvalue, and thus e^{-a_1T} is the spectral radius of e^{TA}. Hence,

$$(sI - \mathrm{e}^{AT})^{-1} = s^{-1}(I - s^{-1}\,\mathrm{e}^{AT})^{-1} = \sum_{k=0}^{\infty} s^{-k-1}\,\mathrm{e}^{kTA},$$

is a nonnegative matrix. In view of (18), this entails that $\psi(s) \ge 1$ for $s > \mathrm{e}^{-a_1T}$. ∎

Proposition 3. *The residual of $\psi(s) = \psi(s|\xi,\eta)$ at the pole $s = \mathrm{e}^{-a_3T}$ is nonnegative, that is,*

$$\lim_{s\to \mathrm{e}^{-a_3T}} \left(s - \mathrm{e}^{-a_3T}\right)\psi(s) \ge 0.$$

In particular, $\psi(s) < 0$ as $s \to \mathrm{e}^{-a_3T} - 0$.

Proof: Applying (34) to $f(z) = f_s(z)$, where

$$f_s(z) \triangleq (sI - \mathrm{e}^{Tz})^{-1}\left(\mathrm{e}^{Tz}\,\xi + z(\mathrm{e}^{-Tz} - 1)^{-1}\eta\lambda\right),$$

and using the definition of J, D, one proves that

$$\psi(s) \overset{(18)}{=} 1 - Cf_s(A)B = 1 - \sum_{i=1}^{3} \bar{c}_i\bar{b}_i\rho_s(-a_i),$$

where $\bar{b}_i, \bar{c}_i$ are the coordinates of the vectors $\bar{B} := S^{-1}B$, $\bar{C} := CS$, and S is the matrix from (31). Obviously, $\rho_s(-a_i)$ exists and is analytic in a vicinity of $s = -\mathrm{e}^{-a_3T}$ for $i = 1, 2$, and hence the residual in question is found as

$$\begin{aligned}\lim_{s\to \mathrm{e}^{-a_3T}} &\left(s - \mathrm{e}^{-a_3T}\right)\psi(s) = \\ &= -\bar{c}_3\bar{b}_3 \lim_{s\to \mathrm{e}^{-a_3T}} \left(s - \mathrm{e}^{-a_3T}\right)\rho_s(-a_3) = \\ &= -\bar{c}_3\bar{b}_3\left(\xi\,\mathrm{e}^{-a_3T} - \eta\lambda a_3(\mathrm{e}^{a_3T} - 1)^{-1}\right).\end{aligned}$$

Using (31) and (32), it is easy to check that, $\bar{c}_3 = 1$ and $\bar{b}_3 = g_1g_2/(a_2 - a_3)(a_1 - a_3) > 0$, and hence the latter expression is nonnegative, since $a_3 > 0$, $\xi \le 0$ and $\eta \ge 0$. ∎

Proposition 4. *The function $c(\eta)$ defined by (19) is strictly decreasing, in particular, $c(\eta) \le c(0) = \mathrm{e}^{-(a_1+a_2+a_3)T}$ for $\eta \ge 0$. Hence, $\psi(c(\eta)|\xi,\eta)$ is well-defined for $\eta \ge 0$.*

Proof: The proof of the first statement is straightforward from Corollary 3, entailing that $CA(I - \mathrm{e}^{AT})^{-1}B < 0$, and taking into account (19). The second statement is obvious by recalling that the poles of ψ are $\mathrm{e}^{-a_iT} > c(\eta)$. ∎

Proposition 5. *If (21) holds, then the number of roots of the polynomial $\chi(s)$ (or, equivalently, the rational function $\psi(s)$) on the interval $(-\infty, -1]$, counted with multiplicity, is 0 or 2.*

Proof: Since $\chi(s) \to -\infty$ as $s \to -\infty$ and $\chi(-1) = -\psi(-1)(1+\mathrm{e}^{-a_1T})(1+\mathrm{e}^{-a_2T})(1+\mathrm{e}^{-a_3T}) < 0$ if (21) holds, the number of sign changes of χ on $(-\infty, -1]$ must be even. Consequently, χ has either no roots or exactly two roots in this interval, which proves the statement. ∎

Necessity of (20) and (21)

We start the proof of Theorem 2 by establishing the following lemma.

Lemma 2. *If matrix $\mathscr{Q}$ is Schur stable, then the conditions (20) and (21) hold.*

Proof: To prove (20), notice that $C\,\mathrm{e}^{-AT}J = CB = 0$ and $C\,\mathrm{e}^{-AT}D = \lambda CA(I - \mathrm{e}^{AT})^{-1}B$. Here, the following equivalent representations of D, J from (14) are used

$$D = \lambda A(\mathrm{e}^{-AT} - I)^{-1}B, \quad J = \mathrm{e}^{AT}B. \tag{38}$$

Hence, $\psi(0) = 1 + \eta\lambda CA(I - \mathrm{e}^{AT})^{-1}B$. On the other hand, $\det\mathscr{Q} = -\chi(0) = \det\mathrm{e}^{AT}\,\psi(0)$ is the product of the eigenvalues of $\mathscr{Q}$. The Schur stability entails (20) in view of the inequalities $|\chi(0)| < 1$ and

$$\psi(0) = -\det\mathrm{e}^{-AT}\,\chi(0) > -\det\mathrm{e}^{-AT} = -\mathrm{e}^{(a_1+a_2+a_3)T}.$$

Inequality (21) is obtained by noticing that, on one hand, $\det(I + \mathrm{e}^{AT}) = (1+\mathrm{e}^{-a_1T})(1+\mathrm{e}^{-a_2T})(1+\mathrm{e}^{-a_3T}) > 0$, and, on the other hand, $\chi(-1) < 0$, since $\chi(s) \to -\infty$ as $s \to -\infty$ and $\mathscr{Q}$ does not have eigenvalues on $(-\infty, 1]$. Hence, $\psi(-1) = -\chi(-1)/\det(I + \mathrm{e}^{AT}) > 0$. ∎

Theorem 2: Non-Critical Case

By virtue of Proposition 4, one has $c(\eta) \in (-\infty, \mathrm{e}^{-a_3T})$, on which interval the function $\psi(s|\xi,\eta)$ is well-defined. Proving Lemma 2, it has been shown that

$$\psi(0|\xi,\eta) = \mathrm{e}^{(a_1+a_2+a_3)T}\,c(\eta).$$

On the other hand, the definition of ψ in (18) implies that

$$\begin{aligned}\det\mathscr{Q}(\xi,\eta) &= -\chi(0|\xi,\eta) \\ &= \psi(0|\xi,\eta)\,\mathrm{e}^{-(a_1+a_2+a_3)T} = c(\eta).\end{aligned}$$

Necessity part. The necessity of (20) and (21) is implied by Lemma 2. To prove the necessity of (22), notice that its violation $\psi(c(\eta))c(\eta) \le 0$ implies that $\psi(c(\eta))\psi(0) \le 0$, that

is, $\psi(s)$ and $\chi(s)$ have a root s_* (i.e., an eigenvalue of $\mathscr{Q}$) lying between 0 and $c(\eta)$. Since $\psi(0) \neq 0$, one has $0 < |s_*| \leq |c(\eta)| = |\det \mathscr{Q}|$, entailing that the product of two other eigenvalues of $\mathscr{Q}$ should be at least 1 in modulus. Hence, violation of (22) is incompatible with the Schur stability of $\mathscr{Q}$. The necessity part is proven.

Sufficiency part. Assume now that (20), (21), and (22) hold. It will be proven that $\mathscr{Q}$ has one real eigenvalue $s_1 \in (-1, \mathrm{e}^{-a_3 T})$, whereas two other of its eigenvalues $s_2, s_3 \in \mathbb{C}$ satisfy the condition $0 < s_2 s_3 < 1$.

Indeed, if $c(\eta) > 0$, one has $\psi(c(\eta)) > 0$ and, by virtue of Proposition 3, $\psi(s)$ has a root $s_1 \in (c(\eta), \mathrm{e}^{-a_3 T})$, being an eigenvalue of $\mathscr{Q}$. On the other hand, if $c(\eta) < 0$, then (20) entails that $c(\eta) > -1$. Due to (21) and (22), entailing that $\psi(-1) > 0 > \psi(c(\eta))$, the matrix $\mathscr{Q}$ has an eigenvalue $s_1 \in (-1, c(\eta))$. In both situations, s_1 has the same sign as $c = \det \mathscr{Q} = s_1 s_2 s_3$ and $|s_1| > |c|$. Hence, $0 < s_2 s_3 < 1$.

If we have a pair of complex-conjugate roots $s_2 = s_3^*$, then $|s_2| = |s_3| = \sqrt{|s_2 s_3|} < 1$. If $s_2, s_3 > 0$, then $s_2, s_3 < \mathrm{e}^{-a_1 T}$ thanks to Proposition 2. Finally, if $s_2, s_3 < 0$, then $s_2, s_3 > -1$ due to Proposition 5 (since, otherwise, $s_2, s_3 \leq -1$ and $s_2 s_3 \geq 1$). Thus, in all possible situations, $\mathscr{Q}$ is Schur stable, having three eigenvalues inside the unit disk.

It has been proven that the spectral radius $\rho(\mathscr{Q})$ of $\mathscr{Q}$ is not less than $|s_1| > |c(\eta)|$. The proof of Theorem 2 in the non-critical case is complete.

Theorem 2: Critical Case

Notice first that $c(\eta) = 0$ if and only if

$$\eta = \eta_* \triangleq -\frac{1}{CA(I - \mathrm{e}^{TA})^{-1} B},$$

where η_* is well-defined and positive (Proposition 4). As has been shown, $\psi(0|\xi, \eta_*) = \det \mathrm{e}^{AT}\, c(\eta_*) = 0$, that is, independent of the choice of ξ, the matrix $\mathscr{Q}$ has eigenvalue at 0. Introducing the derivative

$$\psi'(s|\xi, \eta) \triangleq \frac{\partial \psi}{\partial s}(s|\xi, \eta) = C(sI - \mathrm{e}^{AT})^{-2}(\xi J + \eta D),$$

the condition (23) can be written as $|\psi'(0|\xi, \eta)| < \mathrm{e}^{(a_1+a_2+a_3)T}$. To prove Theorem 2, consider two cases.

Case 1: The matrix $\mathscr{Q}$ has multiple eigenvalue at 0, that is, for a given triple $T > 0$, $\xi \leq 0$, and $\eta = \eta_*$, it holds that $\psi(0) = \psi'(0) = 0$. In this case, (23) is fulfilled automatically. It is established that (21) is necessary for Schur stability. On the other hand, if (21) holds, the third eigenvalue of $\mathscr{Q}$ (which is automatically real) lies between -1 and $\mathrm{e}^{-a_1 T}$ due to Propositions 2 and 5.

Case 2: Assume now that only one of the three eigenvalues $s_1(\eta), s_2(\eta), s_3(\theta)$ vanishes at $\eta = \eta_*$, without loss of generality, assume that $s_1(\eta_*) = 0$. Since this eigenvalue is simple, one has $\psi'(0|\xi, \eta_*) \neq 0$. In view of the implicit function theorem, $s_1(\eta)$ is C^1-smooth in a vicinity of $\eta = \eta_*$. Differentiating the relation

$$\psi(s_1(\eta)|\xi, \eta) = 0$$

with respect to η and substituting $s_1(\eta_*) = 0$, one shows that

$$\frac{ds_1(\eta_*)}{d\eta}\psi'(0|\xi, \eta_*) = -\frac{\partial \psi}{\partial \eta}(0|\xi, \eta) \overset{(18)}{=} C\,\mathrm{e}^{-AT}(\lambda^{-1} D) = \\ = CA(I - \mathrm{e}^{TA})^{-1} B \overset{(19)}{=} \mathrm{e}^{(a_1+a_2+a_3)T}\,\frac{dc(\eta_*)}{d\eta}.$$

Recalling that $\det \mathscr{Q}(\xi, \eta) = c(\eta)$ and applying the L'Hôpital rule leads to

$$\lim_{\eta \to \eta_*} s_2(\eta) s_3(\eta) = \lim_{\eta \to \eta_*} \frac{c(\eta)}{s_1(\eta)} = \frac{dc(\eta_*)/d\eta}{ds_1(\eta_*)/d\eta} \\ = \mathrm{e}^{-(a_1+a_2+a_3)T}\,\psi'(0|\xi, \eta_*).$$

Hence, (23) is equivalent to the inequality $|s_2(\eta_*) s_3(\eta_*)| < 1$, which is necessary for the Schur stability of $\mathscr{Q}(\xi, \eta_*)$, whereas the necessity of (21) is ensured by Lemma 2.

On the other hand, if $|s_2(\eta_*) s_3(\eta_*)| < 1$ and (21) hold, then, similar to the proof of non-critical case, one shows that either $s_2(\eta_*) = \bar{s}_3(\eta_*)$ (and their modulus is thus less than 1) or $s_2(\eta_*), s_3(\eta_*) \in (-1, \mathrm{e}^{-a_1 T})$. Since $s_1(\eta_*) = 0$, the matrix $\mathscr{Q}$ is Schur stable. This proofs the sufficiency part.

Appendix D
Eigenvalues of $Q'(X)$: Amplitude Modulation Case

The entries of the matrix exponential in (3) (see Appendix A) are

$$\mathrm{e}^{At} = \tag{39}$$
$$\begin{bmatrix} \mathrm{e}^{-a_1 t} & 0 & 0 \\ g_1 t\,\mathrm{e}[-a_1 t, -a_2 t] & \mathrm{e}^{-a_2 t} & 0 \\ g_1 g_2 t^2\,\mathrm{e}[-a_1 t, -a_2 t, -a_3 t] & g_2 t\,\mathrm{e}[-a_2 t, -a_3 t] & \mathrm{e}^{-a_3 t} \end{bmatrix},$$

and the vector $J = \mathrm{e}^{TA} B$ is the first column of the exponential. Using these facts, the following proposition is straightforward.

Proposition 6. *The characteristic polynomial of $Q'_F(X)$ is*

$$\chi(s) = s^3 - \gamma_1 s^2 - \gamma_2 s - \gamma_3 = 0, \tag{40}$$

where

$$\gamma_1 = \mathrm{e}^{-a_1 T} + \mathrm{e}^{-a_2 T} + \mathrm{e}^{-a_3 T} \\ + F'(\bar{y}_0) g_1 g_2 T^2\,\mathrm{e}[-a_1 T, -a_2 T, -a_3 T],$$
$$\gamma_2 = F'(\bar{y}_0) g_1 g_2 T^2 \left(\mathrm{e}[-a_1 T, -a_2 T]\,\mathrm{e}[-a_2 T, -a_3 T] \right. \\ \left. - \mathrm{e}^{-a_2 T}\,\mathrm{e}[-a_1 T, -a_2 T, -a_3 T]\right) - \mathrm{e}^{-a_1 T}(\mathrm{e}^{-a_2 T} + \mathrm{e}^{-a_3 T}) \\ - \mathrm{e}^{-(a_2+a_3)T},$$
$$\gamma_3 = \mathrm{e}^{-(a_1+a_2+a_3)T}.$$

Notice that at the bifurcation point, where two eigenvalues are equal $\lambda_1 = \lambda_2$, one has

$$\chi(s) = (s - \lambda_1)^2 (s - \lambda_3). \tag{41}$$

The roots of the characteristic polynomial at the bifurcation point are thus calculated as

$$\xi_1 = -\frac{\gamma_1}{2} = \sqrt{\gamma_2}, \quad \xi_3 = -\frac{\gamma_3}{\gamma_2}.$$

The achievable spectral radius of the Jacobian is $\max(|\xi_1|, |\xi_3|)$. The slope tangent $F'(\bar{y}_0)$, corresponding to this bifurcation point, in turn, can be found from the relation between γ_1 and γ_2.